NPL
National Physical Laboratory

Report

NPL REPORT
DQL-RD 004

The NPL air kerma primary standard TH100C for high dose rate ^{192}Ir brachytherapy sources

T Sander and R F Nutbrown

NOT RESTRICTED

OCTOBER 2006

dti

The DTI drives our ambition of 'prosperity for all' by working to create the best environment for business success in the UK. We help people and companies become more productive by promoting enterprise, innovation and creativity.

We champion UK business at home and abroad. We invest heavily in world-class science and technology. We protect the rights of working people and consumers. And we stand up for fair and open markets in the UK, Europe and the world.

The National Physical Laboratory is operated on behalf of the DTI by NPL Management Limited, a wholly owned subsidiary of Serco Group plc

The NPL air kerma primary standard TH100C for high dose rate ^{192}Ir brachytherapy sources

T Sander and R F Nutbrown
Quality of Life Division

ABSTRACT

In 2002 a project was started at the National Physical Laboratory with the aim to set up a new calibration service for dosemeters used to determine the reference air kerma rate of high dose rate ^{192}Ir brachytherapy sources. This report details the construction and the commissioning of the spherical graphite-walled cavity ionisation chamber and the associated measurement set-up which was established as the UK national primary standard for ^{192}Ir in May 2004.

ISSN 1744-0637

National Physical Laboratory
Hampton Road, Teddington, Middlesex, TW11 0LW

Approved on behalf of Managing Director, NPL, by
Simon Duane, Knowledge Leader, Radiation Dosimetry

Table of contents

1 Introduction

The National Physical Laboratory (NPL) has established a spherical graphite-walled cavity ionisation chamber (serial number: TH100C) as the UK national air kerma primary standard for the direct measurement of ^{192}Ir gamma rays.
At present, ^{192}Ir is the most commonly used radioisotope for high dose rate (HDR) brachytherapy treatment (Das and Thomadsen 2005). Due to the relatively short half-life of ^{192}Ir (73.827 days ± 0.013 days) (DDEP 2005), most radiotherapy departments change their ^{192}Ir sources every three months and medical physicists need to measure the source strength of the ^{192}Ir sources on a regular basis before an accurate treatment plan can be written.
In Europe, the recommended quantity for the specification of brachytherapy gamma ray sources is the reference air kerma rate (RAKR), defined by the International Commission on Radiation Units and Measurements (ICRU 1985, ICRU 1997) as the kerma rate to air, in air, at a reference distance of 1 metre, corrected for air attenuation and scattering. The RAKR can be expressed by the following equation:

$$\dot{K}_R = \dot{K}_{air}(d) \cdot \left(\frac{d}{d_{ref}} \right)^2 \qquad (1)$$

where $\dot{K}_R$ is the reference air kerma rate (Gy s^{-1}), $\dot{K}_{air}$ is the air kerma rate (Gy s^{-1}) measured at distance d, which is the distance (m) from the centre of the source to the centre of the primary standard ionisation chamber and d_{ref} is the reference distance of 1 m. The ICRU 1985 report also states that for cylindrical sources, the direction from the source centre to the reference point shall be at right angles to the long axis of the source.

Until the development of the NPL primary standard chamber for ^{192}Ir, the problem in deriving an air kerma calibration coefficient for ^{192}Ir dosemeters was the fact that many parts of the photon (gamma and X-ray) spectrum of ^{192}Ir fall in an energy gap between energy ranges covered by the primary standards for X-rays (free-air chambers) and ^{137}Cs and ^{60}Co gamma rays (cavity chambers) established at primary standard laboratories (IAEA 2002). Free-air chambers are suitable for the measurement of X-rays up to 300 keV (Attix 1986) and the cavity chambers already established at many primary standard laboratories were designed for the measurement of ^{137}Cs and ^{60}Co sources with average photon energies of 662 keV and 1250 keV, respectively. The exposure-weighted average energy of all ^{192}Ir lines is 356 keV. Removing the two strong *L* X-ray lines (9.00 keV and 9.44 keV), which are almost completely attenuated by the source encapsulation, results in a weighted average of 397 keV (Goetsch *et al.* 1991). When no primary standard was available for the direct measurement of HDR ^{192}Ir sources, the air kerma calibration coefficient for ^{192}Ir was determined by using interpolation techniques.
Various methods for the calibration of ^{192}Ir HDR sources have been described in the literature. Goetsch *et al.* (1991) derive the calibration coefficient of an Exradin model A3 ionisation chamber by linear interpolation between the ^{137}Cs gamma-ray energy and the average energy (146 keV) of a 250 kVp, medium filtered X-ray beam (HVL =

3.2 mm Cu), with a correction for the differences in wall attenuation between X-ray, ^{137}Cs and ^{192}Ir irradiation. The calibration jig used for the standard Goetsch technique has been improved recently (Stump *et al.* 2002). An uncertainty analysis was performed and the total expanded uncertainty (k = 2) of the source calibration was calculated to be 2.15%.

Aird *et al.* (1993) recommend that the calibration coefficient of a thimble chamber for use with ^{192}Ir should be that for the highest available kilovoltage quality, i.e. for heavily filtered 280 kVp therapy level X-rays (HVL = 4.0 mm Cu). The expanded uncertainty of the chamber calibration coefficient at 280 kVp quoted by the NPL is 1.2% (k = 2). Due to the extrapolation of the calibration curve to 397 keV, it is difficult to estimate the additional uncertainty.

Büermann *et al.* (1994) developed a method where the traceability to primary standards is maintained by calibrating a suitable ionisation chamber in the reference fields for X-rays up to 300 kVp, ^{137}Cs and ^{60}Co gamma rays. Due to the continuous X-ray spectrum, the response function has to be unfolded to a monoenergetic function prior to the interpolation of the calibration coefficient. The procedure comprises the evaluation of the entire calibration function of the ionisation chamber between 20 keV and ^{60}Co gamma radiation, and an interpolation for the ^{192}Ir emission lines weighted with their emission probability. The overall uncertainty in the determination of the reference air kerma rate of an HDR ^{192}Ir source using a 1000 cm^3 LS-01 chamber was found to be 2.4% (k = 2).

Petersen *et al.* (1994) describe two methods for the derivation of ^{192}Ir calibration coefficients for thimble-type ionisation chambers (type NE2561 and NE2571).

Using the first method, the chambers were calibrated against the NMi (The Netherlands' Measurements Institute) primary standards for X-rays, ^{137}Cs and ^{60}Co gamma radiation and the calibration coefficients of the ionisation chambers were obtained by weighting the chamber response (inverse of the calibration coefficient) according to the air kerma spectrum of the ^{192}Ir source. The X-ray qualities used were the heavily filtered ISO narrow series (ISO 1979). The total expanded uncertainty (k = 2) in the chamber calibration coefficient for ^{192}Ir was estimated to be 1% for the NE2561 chamber and 1.1% for the NE2571 chamber. It should be noted that the quoted overall uncertainty in the chamber calibration coefficients for the highest X-ray energy and for ^{137}Cs and ^{60}Co was of the same order.

This calibration method was compared to a simple averaging of calibration coefficients for ^{137}Cs and a medium filtered X-ray beam (250 kV, 2.94 mm Cu HVL).

For the second method, the total expanded uncertainty (k = 2) of the chamber calibration coefficient was estimated to be 1.5%.

Douysset *et al.* 2005 use a method which is based on the Goetsch method. The RAKR of the ^{192}Ir source was determined using an NE2571 Farmer-type thimble chamber with a calibration coefficient derived from measurements in 250 kV X-rays, ^{137}Cs and ^{60}Co gamma radiation. The RAKR measurement was made by rotating the chamber around the ^{192}Ir source (on a precisely know radius) and by deriving the source-to-chamber distance from the current versus angle curve. The expanded uncertainty (k = 2) in the source calibration is 1.2%.

For all calibration methods described above, the traceability route to primary standards was maintained through external beam secondary standards.

The NPL calibration method for ^{192}Ir HDR sources was developed to offer direct traceability to a primary standard which would potentially reduce the overall measurement uncertainty. The ^{192}Ir source was calibrated against the NPL primary standard cavity chamber TH100C (described in this report) and the calibrated source

was then used to calibrate suitable ionisation chambers, i.e. well chambers or thimble chambers. The expanded uncertainties (k = 2) were estimated to be 0.7% in the ^{192}Ir source calibration using the NPL method, 0.8% in the well chamber calibration coefficient and 1.1% in the thimble chamber calibration coefficient.

2 Construction of the cavity chamber

2.1 General description

The NPL cavity chamber TH100C (see Figure 1) is a guarded ionisation chamber, resulting in low leakage currents and post-irradiation effects.

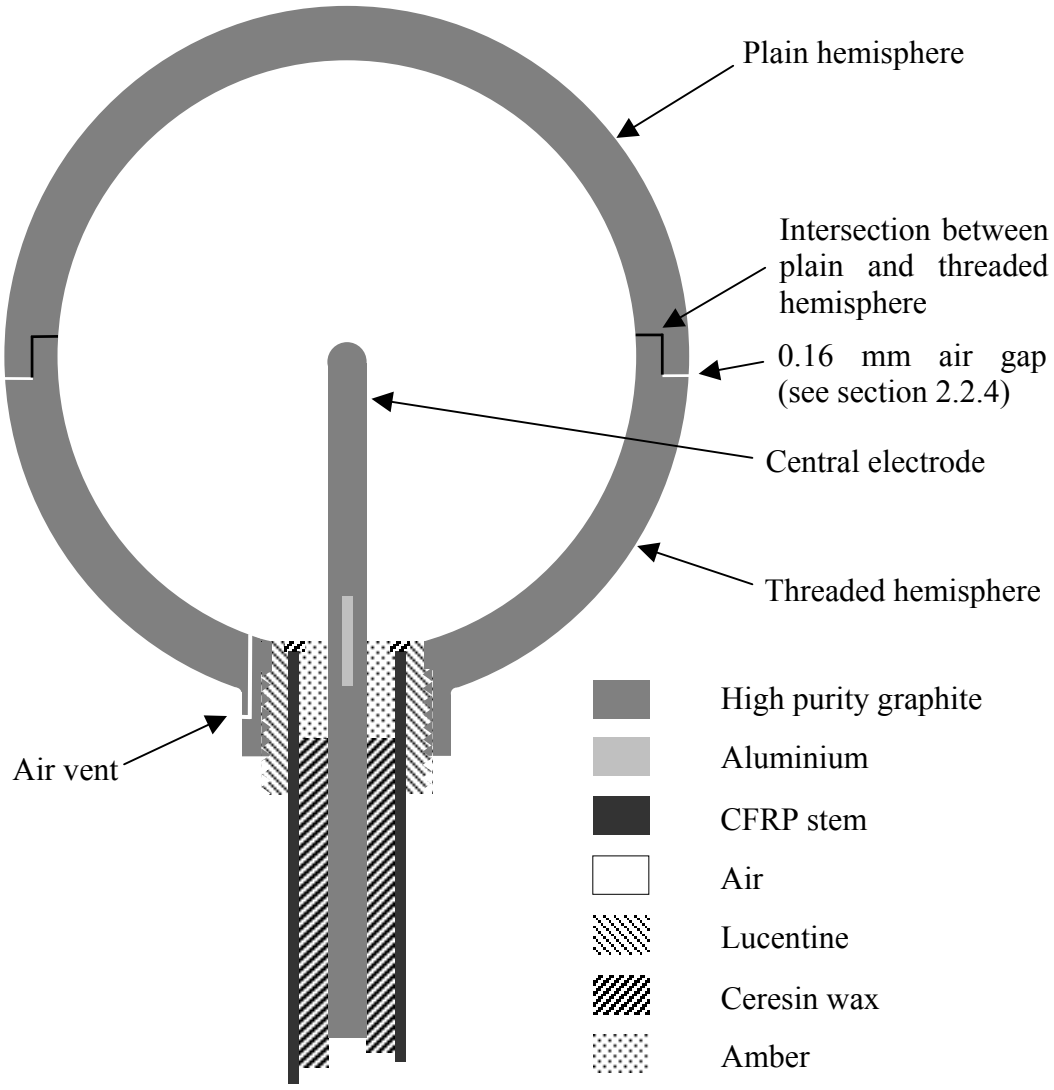

Figure 1. Schematic of the NPL primary standard cavity chamber TH100C (not to scale)

The chamber was originally designed to be a high-energy transfer standard for protection level calibrations. Photon dosimetry requires that an ionisation chamber's

wall thickness must be sufficient to provide charged particle equilibrium (CPE) for the highest energy of secondary electrons present. In the absence of high-energy photoelectrons, the minimum chamber wall thickness required for CPE is that just sufficient to stop maximum-energy Compton recoil electrons. In case of ^{192}Ir this requires a wall thick enough to stop 687 keV electrons generated by 885 keV gamma rays, the most energetic photons emitted by ^{192}Ir (Goetsch *et al.* 1991). The CSDA (continuous slowing down approximation) range of 687 keV electrons is 0.31 g/cm^2 of graphite (ICRU 1984), which is equivalent to a wall thickness of approximately 1.8 mm. The graphite wall of the NPL cavity chamber is between 3.5 mm and 4 mm thick, i.e. there is sufficient build-up material in the chamber wall to provide CPE.

The collecting volume of the chamber is large enough to produce an ionisation current in the order of a few pA if the chamber is used to measure high dose rate ^{192}Ir brachytherapy sources with nominal activities in the order of 370 GBq at a source to chamber distance of approximately 1.4 m.

The graphite used in the cavity chamber (central electrode and both graphite hemispheres) was 'RW-O' spectroscopic grade graphite, a high purity, high strength material manufactured by Ringsdorff-Werke GmbH, Bonn-Bad Godesberg, Germany. The ash content of this type of graphite is 2 ppm and the mean density of the graphite is quoted as 1.75 g cm^{-3} on the data sheet. The density of the graphite was not measured at NPL and therefore a type B uncertainty of 0.03 g cm^{-3} (k = 2) was assigned to the published value. This is 1.7% of the quoted density. As the wall correction for the cavity chamber is 4.53%, an additional type B uncertainty (k = 2) of 0.08% (i.e. 1.7% of 4.53%) was added to the uncertainty budget. The uncertainty in the wall correction factor includes the uncertainty in the wall thickness.

The chamber stem (guard) is made of electrically conducting carbon fibre reinforced plastic (CFRP). A threaded insulating tube made of Lucentine, a styrene-based copolymer, similar to polystyrene in density and effective atomic number, was glued to the top of the chamber stem and the threaded graphite hemisphere was screwed onto the Lucentine tube.

The chamber stem protects the central carbon electrode. The gap between the two components was filled with an electrically insulating material, i.e. Ceresin wax (manufactured by Fisher Scientific UK Limited). At the top end of the chamber stem amber was used to insulate the central electrode from the CFRP stem and Ceresin wax was used to fill the gap between the amber and the threaded Lucentine tube and to insulate the chamber stem from the collecting volume of the cavity chamber.

2.2 Length metrology

The individual components of the cavity chamber assembly were measured in the Centre for Basic, Thermal and Length Metrology (CBTLM) at NPL on two co-ordinate measuring machines (CMMs). The diameter of the graphite hemispheres and the distance of the centre of the hemisphere from the rim of the hemispheres (see Figures 2 and 3) were measured on a CMM fitted with a contacting probe system. The probe system was fitted with a three-millimetre diameter stylus and contacted the surfaces to be measured with a force of 0.05 N. The remaining parameters were measured on a CMM fitted with an optical imaging system. Additional support measurements were made on laboratory standards using the optical imaging CMM. The dimensions of all components and the associated measurement uncertainties can be found in the NPL calibration certificate (ref.: E02080163) and the results are summarised in the next three sections. The mean values obtained from the contacting

and non-contacting CMMs, expressed to the nearest 0.001 mm and referred to a temperature of 20 °C, are given in Tables 1, 2 and 3.

2.2.1 The plain hemisphere

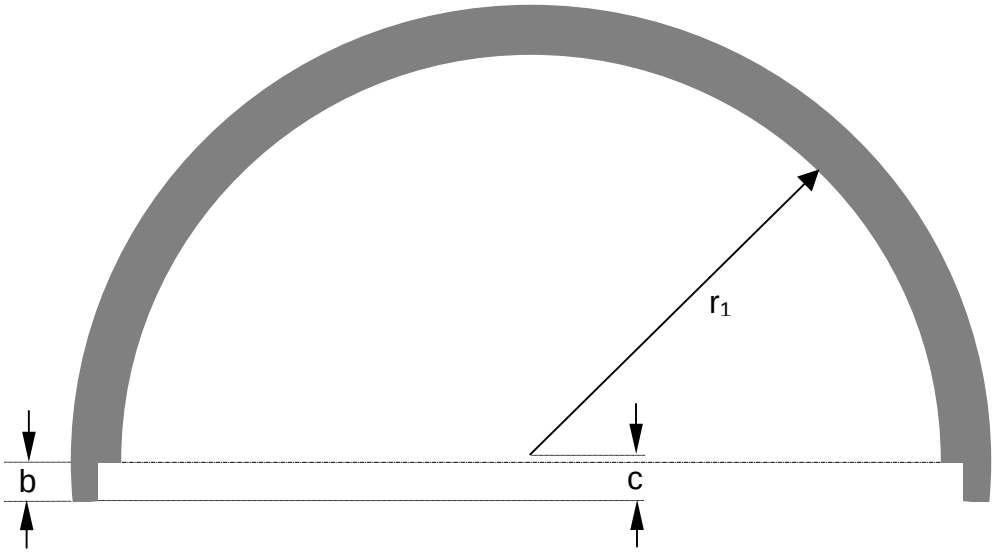

Figure 2. Schematic of the plain hemisphere (not to scale)

Table 1. Dimensions of plain hemisphere and measurement uncertainties ($k = 2$)

Internal diameter = 2 × r_1 (mm)	Depth of upper recess = b (mm)	Distance of hemisphere centre below top surface = c (mm)
58.040 ± 0.033	1.930 ± 0.019	2.038 ± 0.028

2.2.2 The threaded hemisphere

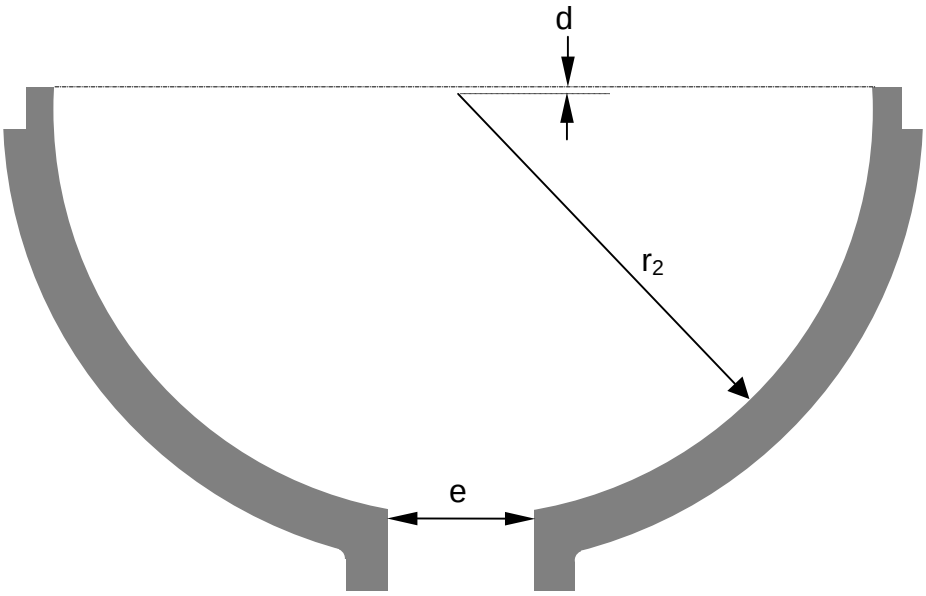

Figure 3. Schematic of the threaded hemisphere (not to scale)

Table 2. Dimensions of threaded hemisphere and measurement uncertainties ($k = 2$)

Internal diameter = $2 \times r_2$ (mm)	Distance of hemisphere centre below top surface = d (mm)	Diameter of hole in hemisphere = e (mm)
58.027 ± 0.033	0.052 ± 0.028	12.040 ± 0.002

The wall thickness of the two hemispheres was measured with a TRIMOS vertical height gauge (type 500, serial number 2438, owned by CBTLM at NPL). The graphite hemispheres were held between two contacting probes. A 3 mm diameter ruby ball was attached to the tip of both styluses. The inside surface of the graphite shell was positioned on a fixed stylus and the upper stylus was lowered onto the outside surface of the graphite shell. The thickness of the plain hemisphere and the threaded hemisphere were measured at the latitudinal positions shown in Figures 4 and 5.
The calibration of the height gauge was checked by measuring the thickness of a 3.500 mm gauge block (s/n 08325) and a 4.000 mm gauge block (s/n L28926, U261). On all occasions the displayed thickness was within ±0.001 mm of the nominal thickness of the gauge blocks. Five thickness measurements were taken equally spaced at each latitudinal position (1 to 10) and the mean thicknesses and the standard deviations of the mean (SDOM) are summarised in Table 3.

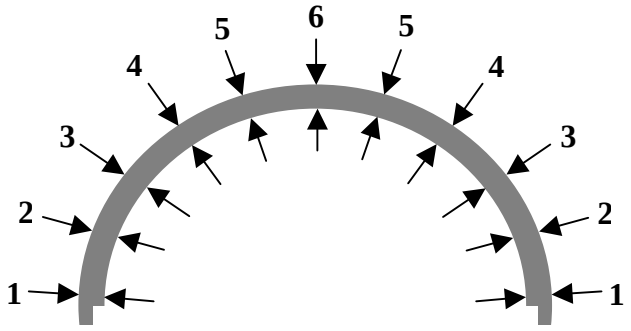

Figure 4. Approximate latitudinal positions of the contacting probes of the vertical height gauge on the plain hemisphere (not to scale)

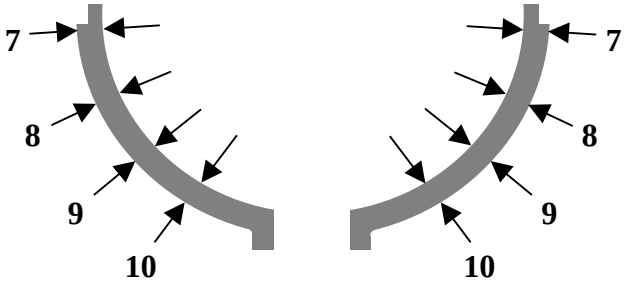

Figure 5. Approximate latitudinal positions of the contacting probes of the vertical height gauge on the threaded hemisphere (not to scale)

Table 3. Wall thickness of plain and threaded hemisphere

Position	Mean wall thickness (mm)	SDOM (%)
1	3.910	0.30
2	3.866	0.14
3	3.761	0.08
4	3.648	0.22
5	3.593	0.04
6	3.562	0.16
7	4.007	0.06
8	3.909	0.10
9	3.755	0.04
10	3.676	0.09

The variation in wall thickness was taken into account for the Monte Carlo simulation of this chamber.

2.2.3 The air gap between the graphite hemispheres

The spherical graphite shell was made of two parts, allowing access to the central electrode. The spherical shell was assembled by pushing the plain hemisphere onto the threaded hemisphere such that the flat surfaces of the inner annular rims (see dash-dotted lines in Figures 2 and 3) were in contact, leaving a 0.16 mm gap (mean value) between both outer rims. The gap width was measured on a CMM (type SIP 414 M, serial number 0510, owned by CBTLM) fitted with an optical imaging system. Four equally spaced measurement points along the gap were chosen at 0º, 90º, 180º and 270º. At each measurement point the gap width was measured three times and the mean gap width was calculated. The plain hemisphere was then removed, pushed back onto the threaded hemisphere and the gap width measurements were repeated. In the first case the mean gap width was found to be 0.1660 mm and in the second case the mean gap width was found to be 0.1524 mm. The difference of 0.0136 mm between the two mean gap widths is equivalent to a change of the internal air volume of the cavity chamber by $V_{cylinder} = \pi \cdot (2.90168\,\mathrm{cm})^2 \cdot 0.00136\,\mathrm{cm} = 0.036\,\mathrm{cm}^3$ which is 0.035% of the calculated internal air volume (see section 2.2.6). This additional uncertainty in the measurement volume was added to the uncertainty budget.

Should it become necessary to take the spherical graphite electrode apart, the gap width will have to be measured after reassembling the sphere and it should be confirmed the measured gap width is within the range 0.1524 mm and 0.1660 mm.

For the RAKR measurements of the ^{192}Ir sources, the long axis of the ionisation chamber was set up perpendicular to the collimated photon beam (see Figure 8) and as the wall thickness of the sphere behind the air gap was only 2 mm, it was decided to investigate whether or not an ‘air gap correction’ had to be applied to the primary standard measurements. Monte Carlo simulations revealed that the air gap correction was negligible. CPE still applies for measurements of ^{192}Ir sources, even with the reduced wall thickness of 2 mm (see section 2.1).

2.2.4 The central electrode

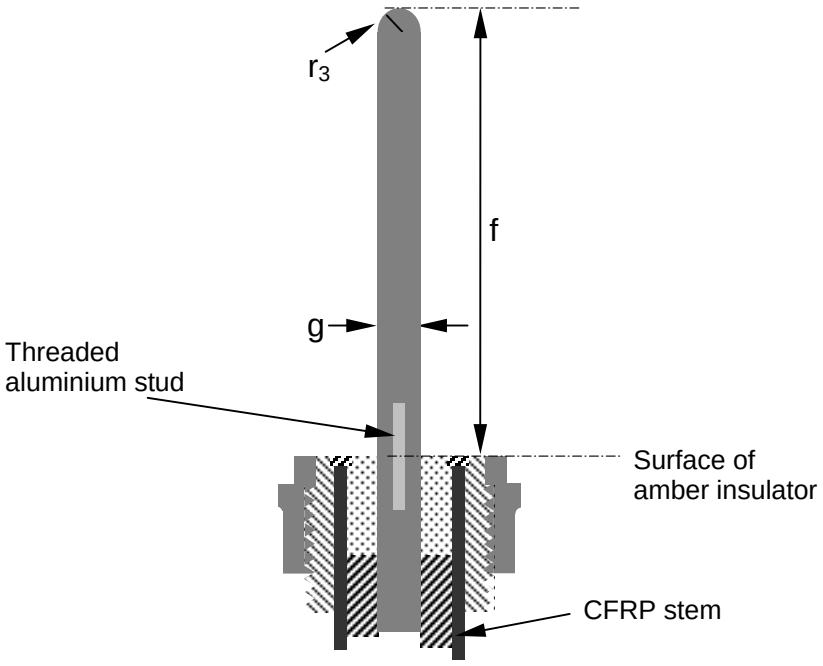

Figure 6. Schematic of the central electrode (not to scale)

Table 4. Dimensions of central electrode and measurement uncertainties ($k = 2$)

Top of central electrode to shoulder = f (mm)	Diameter of central electrode = g (mm)	Radius of electrode top = r_3 (mm)
28.541 ± 0.036	3.056 ± 0.005	1.537 ± 0.006

The pin shaped high purity graphite central electrode of length f was attached to the high purity graphite rod in the chamber stem via a 10 mm long, 1 mm diameter, threaded aluminium stud.

2.2.5 The chamber stem

The chamber stem was slightly modified after the dimensions of the chamber assembly were measured in the Centre for Basic, Thermal and Length Metrology. When the ionisation chamber was reassembled it was found that the electrically conducting chamber stem was not insulated against the collecting volume. In addition the CFRP stem and amber protruded slightly into the air volume. Under standard operating conditions, a polarising voltage of +500 V is supplied to the central electrode (collector) and the chamber stem (guard), whereas the graphite sphere is earthed. Without modifications to the original design of the cavity chamber (see Figure 7a), there would have been an electric field inside the chamber cavity not only between the central electrode and the earthed graphite sphere, but also between the top of the chamber stem and the earthed graphite sphere. Some of the negative ions generated inside the chamber volume would have been lost to the stem and would not

have contributed to the collected ionisation current because only the central electrode is connected to the input of the electrometer.

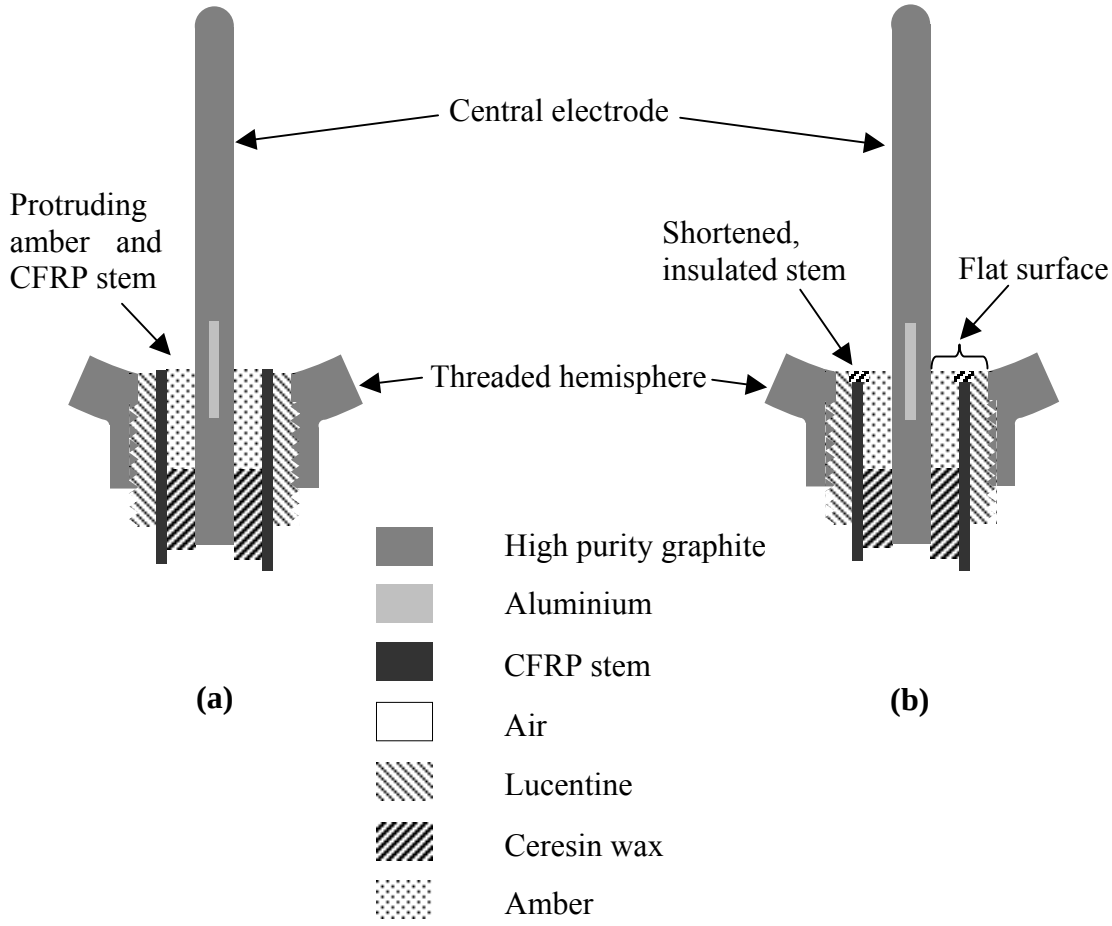

Figure 7. Chamber stem before **(a)** and after **(b)** modification (not to scale)

The top of the electrically conducting CFRP stem was therefore shortened by approximately 1 mm (see Figure 7b) and the Lucentine tube was moved such that the top rim was at the same level as the flat surface of the amber insulator. The gap between the amber insulator and the Lucentine tube was then filled with Ceresin wax.
When the chamber was used as a protection level transfer standard, the effective collecting volume was different from the geometric volume of the air cavity. In order to establish this chamber as an air kerma primary standard, however, the mass of air in the collecting volume, hence the size of the effective collecting volume, had to be known accurately.
Due to the modifications made to the chamber stem, the amber cylinder and the CFRP stem (see Figure 7a) no longer protrude into the internal air volume and the volume of the amber cylinder mentioned in NPL certificate E02080163 must no longer be taken into account when calculating the internal air volume of the cavity chamber.

2.2.6 The collecting volume

The volume was calculated from the dimensions of all components as summarised in sections 2.2.1 to 2.2.4 and was found to be 102.52 cm^3 (BT1 1998 pp 229-232) with a standard uncertainty of 0.09%. An additional type B standard uncertainty of 0.02%

was added due to the possible change in the gap width and hence internal air volume when reassembling the spherical electrode (see section 2.2.3). When the threaded graphite hemisphere was attached to the chamber stem, it was difficult to align the inside surface of the curved electrode exactly with the flat surface of the insulator at the top of the chamber stem. It was assumed that the height of both surfaces would match within ±0.2 mm, which would be equivalent to a volume change of ±5.6 mm^3.
The combined standard uncertainty in the collecting volume was estimated to be 0.09%.

3 Measurement set-up

The experimental set-up for the measurement of reference air kerma rate of an HDR ^{192}Ir brachytherapy source under minimal scattering conditions at a centre-to-centre source-chamber distance (SCD) of 1433 mm is shown in Figure 8 (side view) and Figure 9 (top view).
A lead collimator was designed for use with the HDR brachytherapy source for the following two reasons:
1) to avoid irradiating any air cavities inside the chamber stem and the connectors, which would have resulted in generating an unknown leakage current and 2) to reduce the amount of scattered radiation from the floor and the walls of the exposure room reaching the collecting volume of the cavity chamber and therefore keeping the scatter correction as small as possible.

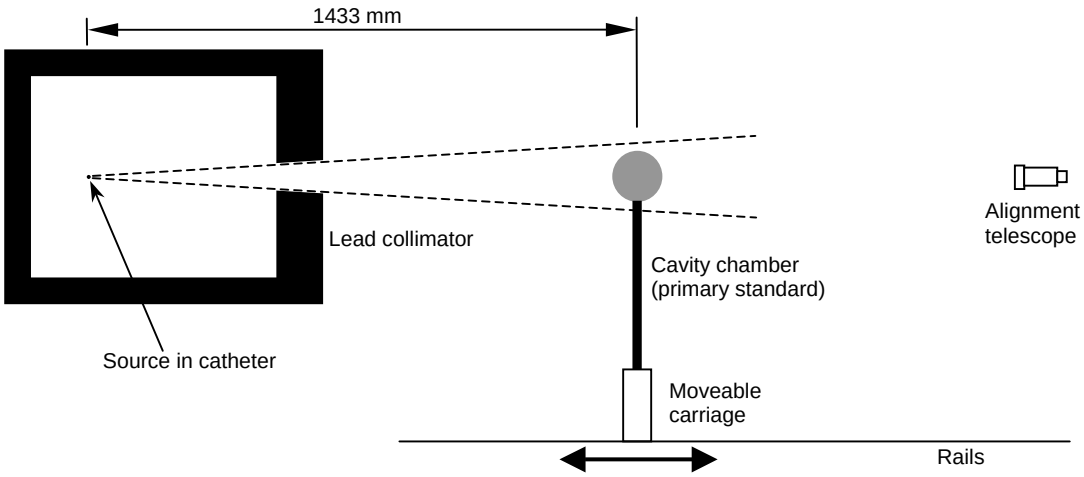

Figure 8. Set-up for ^{192}Ir HDR source calibration at NPL, side view (not to scale)

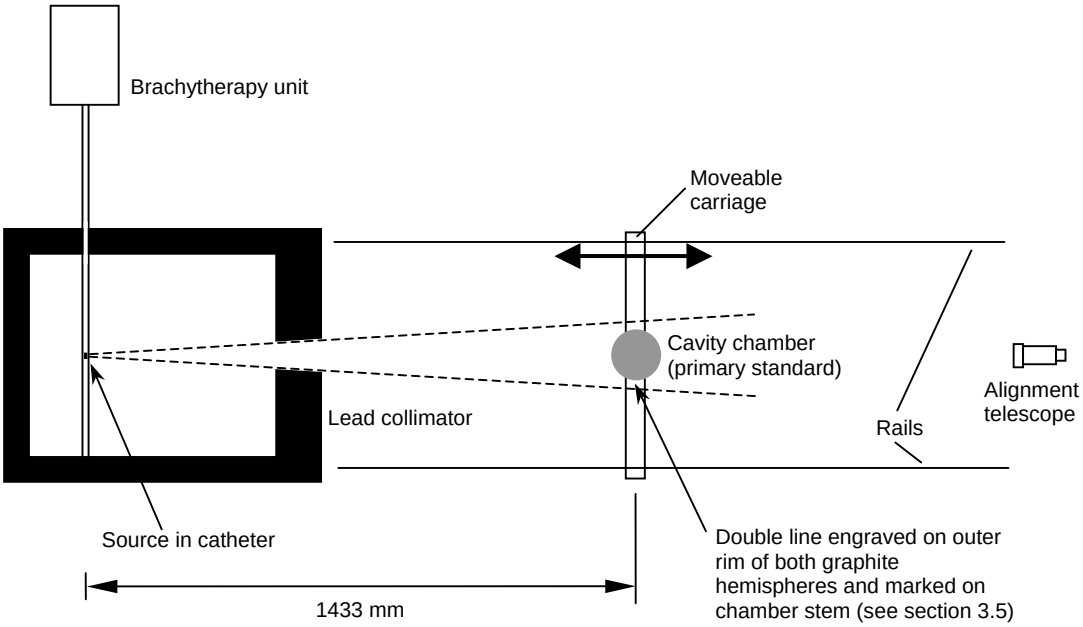

Figure 9. Set-up for ^{192}Ir HDR source calibration at NPL, top view (not to scale)

The lead collimator had to meet the following criteria:
1) As the brachytherapy source is not a point source, the primary photon beam which is emitted through the front face aperture is surrounded by a penumbra. The penumbra should be as small as possible to minimise the scatter correction. This was achieved by moving the source as far away from the aperture as possible.
2) The source should not be in direct contact with the back wall to reduce the contamination of the collimated primary photon beam with fluorescent radiation produced in the lead shielding.
3) The lead castle should not be excessively large and heavy to allow for fine adjustments to be made to the support table holding the assembled lead collimator.
To find a compromise between these three criteria, the ratio of the penumbra and the cross-section of the primary beam at a fixed focal distance was plotted against the source to aperture distance. A suitable distance from the source to the inner surface of the front wall of the lead collimator was found to be 300 mm.

3.1 Estimation of room scatter at point of measurement

The requirement for the thickness of the side walls of the lead collimator was that the dose rate of the gamma rays reflected from the concrete floor and walls should be reduced to less than 0.1% of the dose rate delivered by the primary beam at the point of measurement (centre of ionisation chamber).
Iridium-192 emits photons with discrete energies and the major contributing lines range from 65 keV to 885 keV. A suitable shielding material for the high-energy photons was lead due to its high atomic number and for the following calculation the lead collimator was assumed to have the nominal dimensions listed in Table 5.
The dose rate of gamma rays from ^{192}Ir passing through 40 mm lead (side wall) is reduced to $2E-3$. 75 mm lead (front wall) reduces the dose rate to approximately

5E – 5 (see BS 4094 : Part 1 : 1966, page 28). The number of photons penetrating the front wall of the collimator and then being scattered towards the ionisation chamber was negligible compared to the number of photons in the primary beam. Only the photons penetrating the side walls of the collimator were considered when estimating the reflected dose rate.
The dose rate reflected from a surface may be expressed (Raso 1963) as:

$$\dot{D}_{reflected} = \dot{D}_0 \cos\theta_0 \frac{A}{r^2} \alpha(E_0, \theta_0, \theta, \phi) \qquad (2)$$

where $\dot{D}_{reflected}$ is the reflected dose rate and $\dot{D}_0$ is the dose rate incident on the reflecting surface (here: concrete) at an angle of θ_0 (see Figure 10). A is the reflecting area in m^2, r is the distance from the centre of the reflecting area to the ionisation chamber in m and $\alpha(E_0, \theta_0, \theta, \phi)$ is the dose albedo in % for gammas incident on the reflecting surface where E_0 is the incident gamma energy, θ_0 is the incident angle, θ is the emergent polar angle and ϕ is the emergent azimuthal angle (not shown in Figure 10). ϕ = 0° for forward-scattered radiation (e.g. at point B and C) and ϕ = 180° for backscattered radiation (e.g. at point A and D). The albedo characterises the fraction of radiation scattered at a surface.

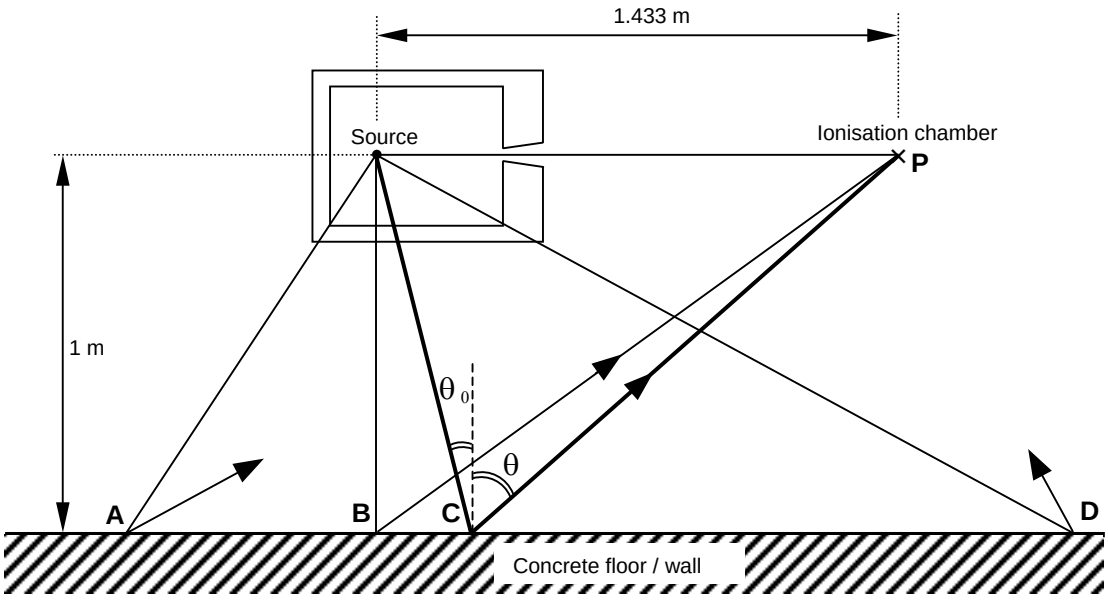

Figure 10. Gamma rays scattered at the concrete floor and walls (not to scale)

For the calculation of the reflected dose rate $\dot{D}_{reflected}$ from the concrete surface, a worst-case scenario was applied in order to overestimate rather than underestimate the reflected dose rate. The ^{192}Ir source was assumed to be set up inside the lead collimator surrounded by a hollow concrete cylinder with an internal radius of 1 m (minimum distance to floor, side walls or ceiling) and the long central axis of the concrete cylinder was assumed to be identical with the axis through the source, the centre of the aperture and the centre of the ionisation chamber (point P in Figure 10).

The reflecting area A was divided into sections corresponding to 10° increments of the incident angle θ_0 between points A and D. For example, the reflecting area between point B ($\theta_0 = 0°$) and C ($\theta_0 = 10°$) is equal to $A = 2\pi \cdot 1 \cdot \overline{BC}$ where $\overline{BC}$ is the length of the hollow concrete cylinder in metres. All individual scatter contributions were added up to estimate the total reflected dose rate. The contribution of gamma rays reflected left of point A ($\theta_0 = -34°$) and right of point D ($\theta_0 = 63°$) was assumed to be negligible. The total reflected dose rate at the point of measurement P was found to be $\dot{D}_{reflected} = \dot{D}_S \cdot (1.7\text{E}-3) \cdot (1/2.5)^2 = \dot{D}_S \cdot 2.7\text{E}-4$ where $\dot{D}_S$ is the dose rate at the source[1]. The inverse square correction was made for a distance of 2.5 m, the minimum total distance from the source to the floor and the floor to the chamber. The dose rate delivered by the primary photon beam at the point of measurement was $\dot{D}_{primary} = \dot{D}_S \cdot (1/1.433)^2 = \dot{D}_S \cdot 4.9\text{E}-1$, i.e. the inverse square correction was made for the standard measurement distance of 1.433 m. The reflected dose rate $\dot{D}$ contributing to air kerma measurements at the point of measurement P was therefore less than 0.1% of $\dot{D}_{primary}$, which means that the chosen wall thickness of 40 mm for the side walls of the lead collimator is sufficient (BT1 1998; pp 243-245).

3.2 Dimensions of the lead collimator

Table 5 summarises the nominal dimensions and the material properties of the lead collimator (NPL Engineering Services drawing number: 99/1054):

Table 5. Nominal dimensions of the lead collimator

Walls	Lead-Antimony Alloy : BS 3909/2 : 1965 (composition: 91% Pb, 9% Sb)
Front face aperture	Wolfmet heavy alloy HA 190 (composition: 90% W, 6% Ni, 4% Cu)
Wall thickness (top, bottom, left, right and back)	40 mm
Front wall thickness	75 mm
Internal length	400 mm
Internal width	300 mm
Internal height	300 mm
External length	515 mm
External width	380 mm
External height	380 mm
Distance from source centre to back wall	100 mm
Distance from source centre to front wall	300 mm
Distance from source centre to side walls (top, bottom, left and right)	150 mm
Diameter of small borehole of conical aperture	20 mm
Opening angle of conical aperture	4.48° ± 0.05°

[1] $\dot{D}_S$ is only a relative number. Here it is equivalent to the dose rate at 1 m.

The lead-antimony walls were manufactured by Fabcast Engineering Limited and the heavy alloy for the front face aperture was supplied by M&I Materials Limited.

3.3 The front face aperture

Figure 11 shows the profile of the conical front face aperture, made of heavy alloy, which was screwed to the front wall of the lead collimator. The borehole had a diameter of x = 20 mm. The active length of the Nucletron microSelectron Classic HDR ^{192}Ir source is 3.5 mm, i.e. it is not a point source. Therefore the primary photon beam outside the lead collimator was surrounded by a penumbra. Assuming a source to front wall distance of 300 mm and an SCD of 1433 mm, the optimum angle of the taper was calculated to be $\alpha = 4.48°$. With these aperture dimensions, scatter from the mouth of the aperture and the penumbra around the primary beam was kept to a minimum.

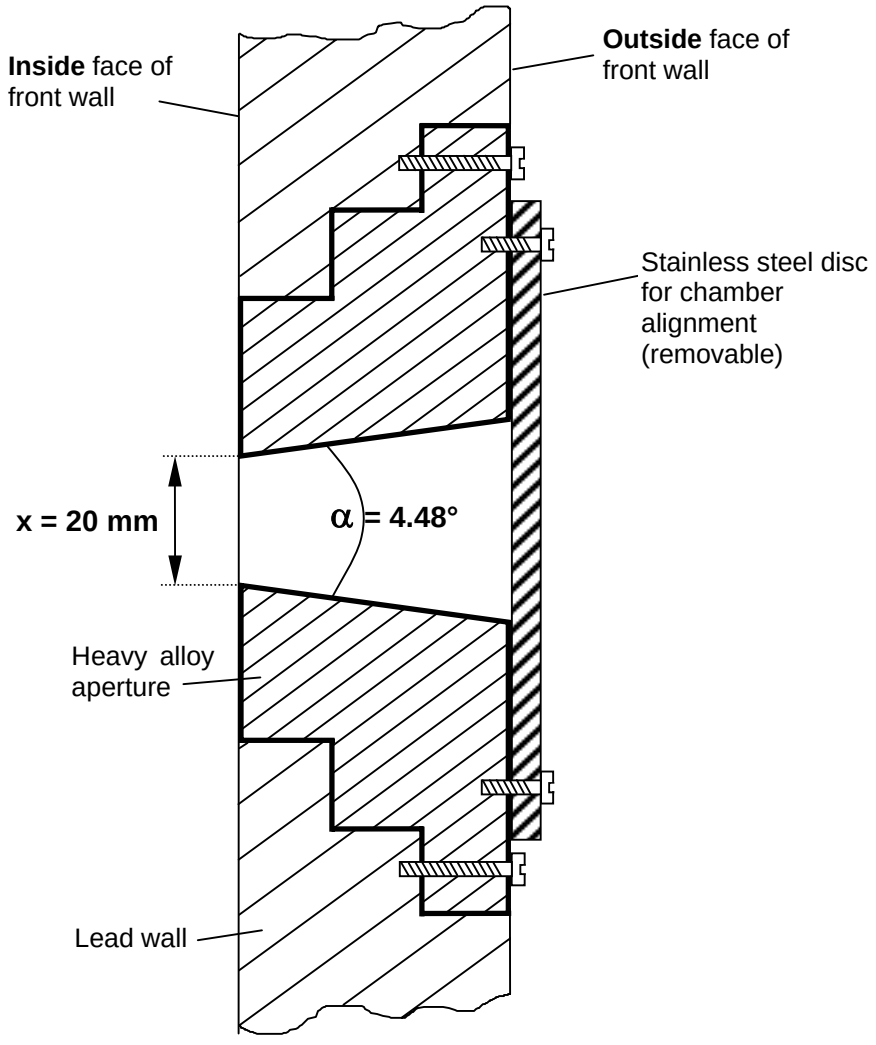

Figure 11. Profile of front face aperture (not to scale)

The diameter of the primary beam with circular cross-section was 82 mm for an SCD of 1433 mm, i.e. if the graphite sphere (66 mm outer diameter) was aligned on the

central beam axis, the collecting volume was fully covered by the primary beam. The maximum diameter of the penumbra was 108 mm. The source to chamber distance and aperture size were chosen to give a uniform field over the whole of the ionisation chamber. Measurements were carried out to investigate the relationship between the chamber and source position and the measured RAKR of the ^{192}Ir source (see section 3.7 – 3.9).
A 5 mm thick stainless steel disc (nominal thickness) was temporarily attached to the outside surface of the 75 mm thick aperture (nominal thickness), see Figure 11. The distance from the outside face of the steel plate to the primary standard cavity chamber (see Figure 12) was measured with a calibrated internal micrometer.

3.4 Scatter within the lead collimator

For RAKR measurements the HDR ^{192}Ir source was set up inside the lead collimator on the long central axis, 10 cm from the back wall. The collimated gamma ray beam was directed towards the primary standard cavity chamber which was set up with the geometric centre of the chamber at a distance of 1.433 m from the centre of the ^{192}Ir source. The long axis of the source was parallel to the floor and perpendicular to the direction of the collimated gamma ray beam (see definition of RAKR in chapter 1).
Ideally the scattered radiation which is produced inside the lead collimator shall not contribute to the primary beam emerging from the aperture. With the chosen dimensions most of the scattered radiation was absorbed within the lead box. Measurements showed that both the amount of scattered radiation emitted through the front face aperture and the scattered radiation produced at the mouth of the aperture were insignificant at the point of measurement.

3.5 Additional features of the lead collimator

A hole of 2.2 mm diameter was drilled through the right side wall of the lead collimator, viewed from the alignment telescope. A 2 mm diameter plastic catheter (Nucletron Lumencath 6F), attached to the brachytherapy treatment unit via a transfer tube, was fed through the hole in the side wall and attached to a vertically adjustable metal pin at the inside surface of the opposite wall. This clamp held the end of the plastic catheter and allowed the end of the tube to be moved to any position ±10 mm vertically above or below the centre. The vertical movement was necessary to ensure the catheter could be aligned on the central beam axis, coincident with the central axis of the conical aperture, after assembling and aligning the lead collimator on the support table (see Figure 8). Another clamp was attached to the outside of the side wall, where the plastic catheter enters the lead collimator. This clamp was used to tauten the plastic catheter once the lid was in place. For the exact position of the centred source relative to the side walls see Table 5.

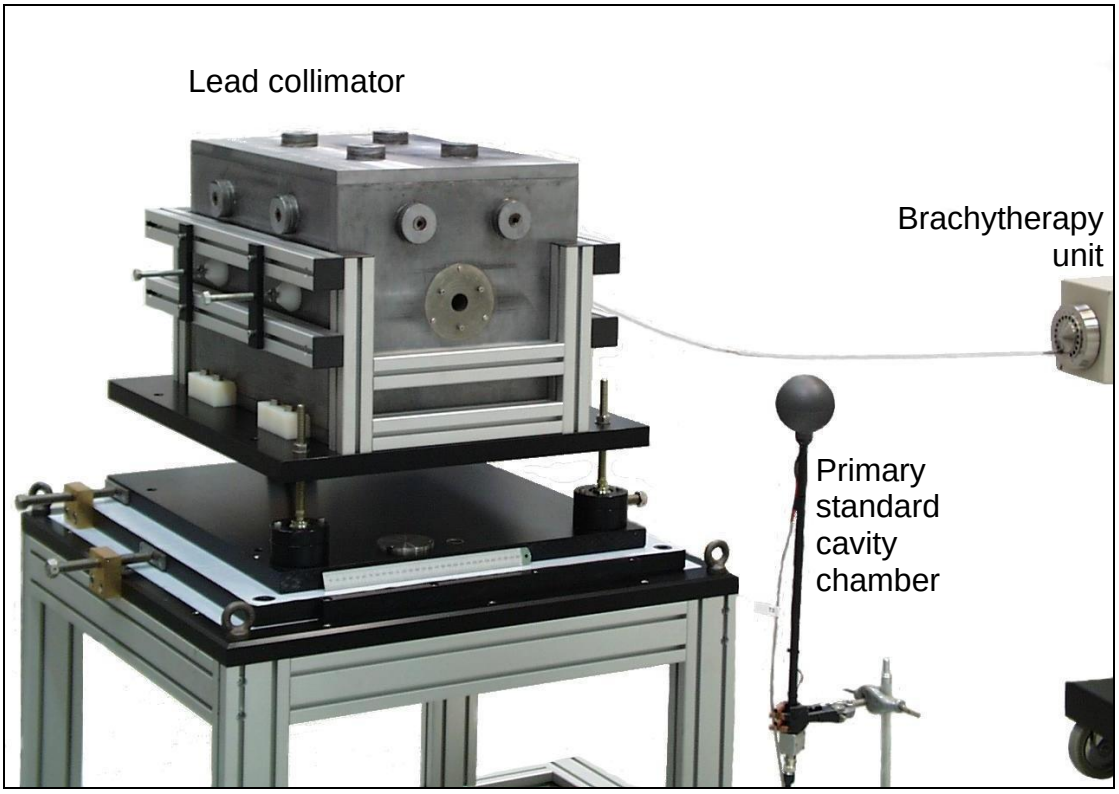

Figure 12. Set-up for ^{192}Ir HDR source calibration at NPL

3.6 Calibration set-up

Before the RAKR of an ^{192}Ir source could be measured, the alignment telescope and the lead collimator were set up in the exposure room as shown in Figures 8 and 9. In order to keep the room scatter to a minimum, it was important to keep the following minimum distances to the concrete walls of the exposure room:

Table 6. Source position relative to the floor, walls and ceiling

Front wall of collimator to opposite exposure room wall	7 m
Back wall of collimator to opposite exposure room wall	1 m
Side walls of collimator to opposite exposure room walls	1 m
Source to floor	1 m
Source to ceiling	1 m

The graphite sphere of the cavity chamber was set up on the central beam axis and rotated so that the double line on the chamber stem pointed towards the left hand side of the movable carriage as viewed from the alignment telescope and as shown in Figure 9. The variation of chamber response with chamber orientation was measured with the double line pointing to four different positions and the results are summarised in Table 7 (BT2 2004; pp 38-41).

Table 7. Variation of chamber response with orientation

Double line pointing towards	RAKR (mGy/h)	SDOM (%)
left (standard position)	47.6795	0.0062
back	47.6571	0.0108
right	47.7027	0.0096
front	47.7196	0.0127
left (standard position)	47.6848	0.0083

The maximum spread between the RAKRs listed in Table 7 was found to be 0.131%. The variation in the measured RAKR with the chamber orientation could be explained with slight variations in the chamber wall thickness (see Table 3). For consistency the ionisation chamber was normally used in the orientation where the measured RAKR was closest to the mean value of the five measurements, i.e. the double line pointed to the left hand side of the carriage, viewed from the telescope.
The centre-to-centre source-chamber distance was set to 1433 mm. Distance a and b (see Table 8) were measured with an internal micrometer after assembling the base plate and the side walls of the collimator and setting up the primary standard cavity chamber.

Table 8. Centre-to-centre source-chamber distance

Half diameter of Lumencath catheter (nominal)	1 mm
Distance from catheter to front face aperture	a mm
Total thickness of front face aperture and steel plate (see Fig. 11)	80.10 mm
Distance from steel plate to front face of graphite sphere	b mm
Mean internal radius of graphite sphere	29.02 mm
Wall thickness of graphite sphere	3.96 mm
Centre-to-centre source-chamber distance	1433.00 mm

The distance from the catheter to the front face aperture could only be measured with the lid of the lead collimator removed. It was estimated that due to the design of the lead collimator this distance would not change by more than ±0.5 mm when the lid was put on top of the collimator. The uncertainty in the length measurement is discussed in chapter 7.

3.7 Source position measurement

After the collimator had been fully assembled, the catheter was tautened with an external clamp. The brachytherapy source was stepped through the catheter while the centre of the ionisation chamber remained stationary on the central beam axis and the measured ionisation current was plotted against the dwell position of the source. Figure 13 shows a typical source position measurement. For the source calibration the dwell position corresponding to the middle of the plateau was chosen. To check the chamber position relative to the primary beam, an X-ray film was placed behind the ionisation chamber and the source was sent to the dwell position mentioned above. The radiograph confirmed that the chamber volume was fully covered by the primary beam.

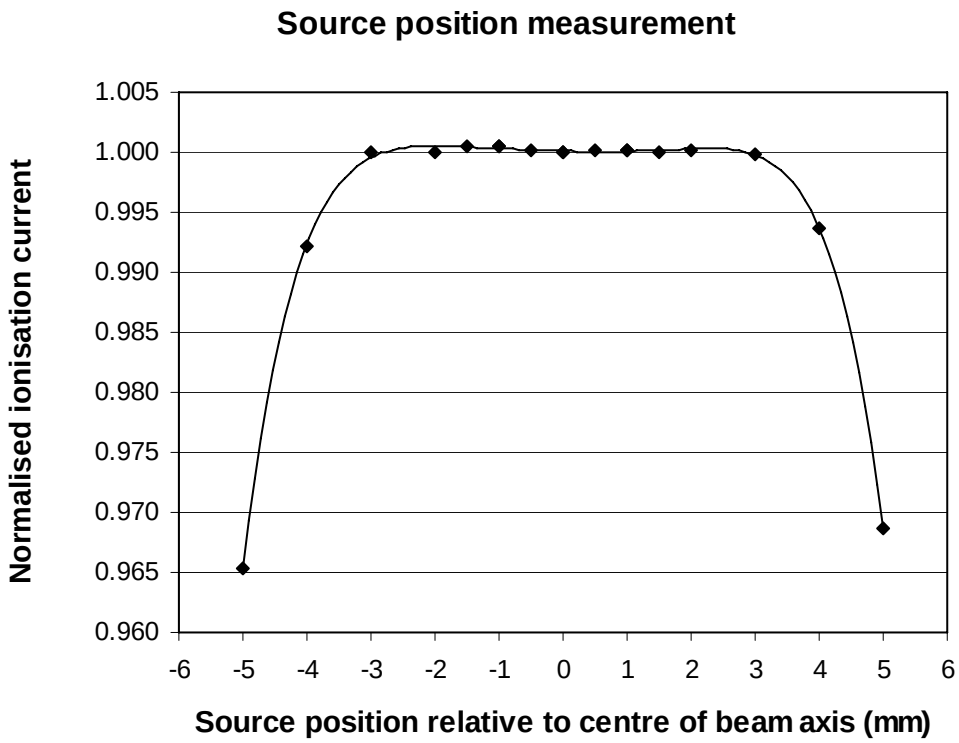

Figure 13. Normalised ionisation current with chamber aligned on central beam axis and source stepping through catheter inside lead collimator

Figure 13 shows that the measured ionisation current, which is proportional to the RAKR, varies by approximately 0.06% if the chamber is aligned on the central axis and the centre of the source is within ±3 mm of the centre. This is well within the overall measurement uncertainty. For dwell positions < -3 mm and > +3 mm, the ionisation current decreases because the chamber is no longer fully covered by the primary beam.

3.8 Horizontal beam profile

The horizontal beam profile was measured by moving the source to the dwell position corresponding to the middle of the plateau of the curve shown in Figure 13. The aligned primary standard chamber was then moved horizontally to ten positions left and right of the centre. Figure 14 shows the variation in the measured ionisation current with chamber position.

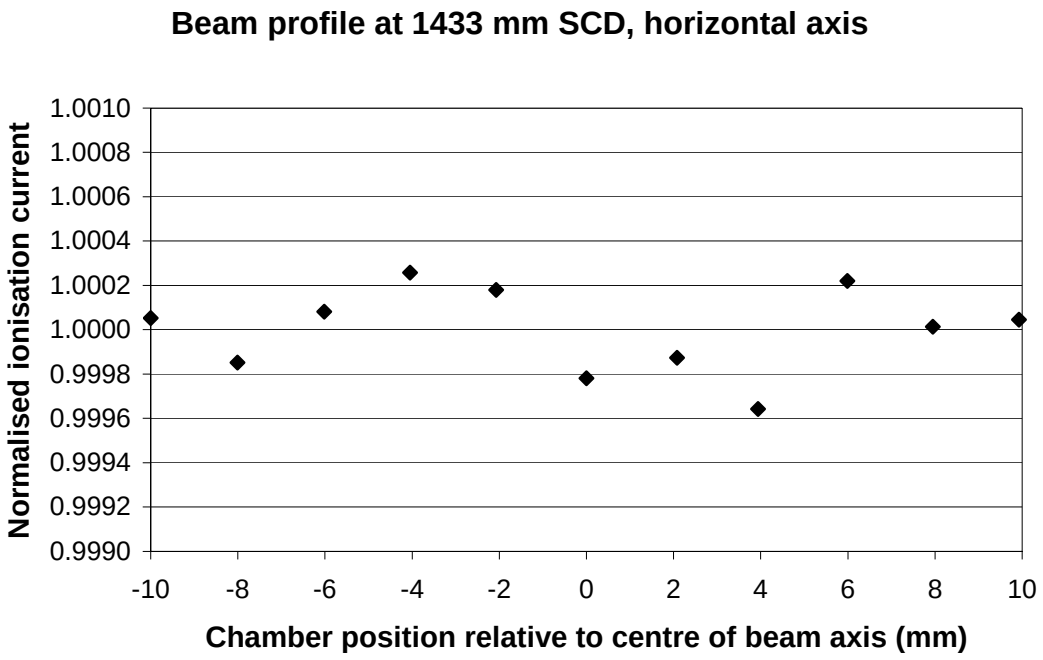

Figure 14. Normalised ionisation current with source aligned on central beam axis and chamber moved horizontally ±10 mm from centre of beam axis

Figure 14 shows that the horizontal positioning of the cavity chamber is not critical as the maximum deviation of the measured ionisation current was found to be only 0.06% if the centre of the ionisation chamber is within ±10 mm of the central axis. This is well within the measurement uncertainty.

3.9 Vertical beam profile

The vertical beam profile was measured by moving the source to the dwell position corresponding to the middle of the plateau. The aligned primary standard chamber was then moved vertically to ten positions above and below the centre. Figure 15 shows the variation in the measured ionisation current with chamber position.

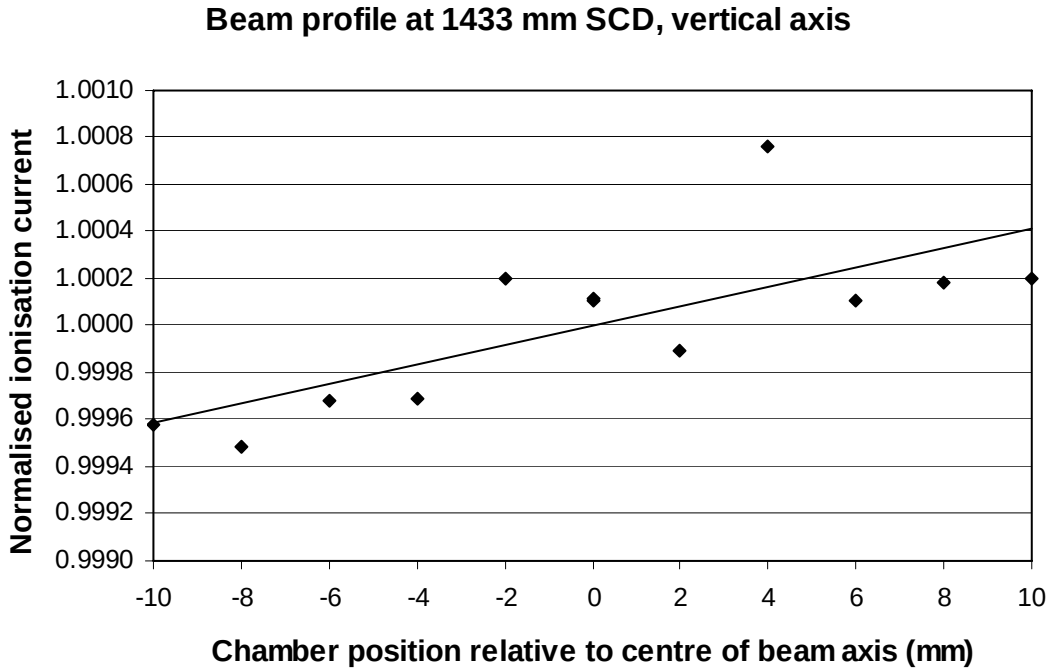

Figure 15. Normalised ionisation current with source aligned on central beam axis and chamber moved vertically ±10 mm below and above centre of beam axis

The data points plotted in Figure 15 show a slight trend. As the spherical electrode is moved upwards, an increasing amount of the threaded boss and chamber stem are exposed to the primary photon beam and the amount of scattered radiation contributing to the measured ionisation current increases. As long as the centre of the graphite sphere is within ±5 mm of the central beam axis, the deviation was found to be within 0.04% (see linear trendline in Figure 15) which is again well within the measurement uncertainty.

4 The correction factors

4.1 Correction factors determined by measurement

4.1.1 Stem scatter correction

The hollow graphite electrode is attached to a 10 mm diameter chamber stem. The sphere is constructed in two halves, the upper hemisphere being removable to allow access to the inner components. The lower hemisphere is screwed onto the chamber stem via a threaded boss. When the chamber is irradiated at the calibration distance of 1433 mm, the radiation field (82 mm diameter) covers not only the whole graphite sphere (66 mm diameter) but also the threaded boss and the top of the chamber stem, leading to an increase in the number of scattered photons reaching the collecting volume and therefore an increase in the measured ionisation current. A dummy stem made of the same materials and having the same dimensions as the chamber stem was used to measure the stem scatter correction. The top of the dummy stem was positioned opposite the chamber stem (see Figure 16).

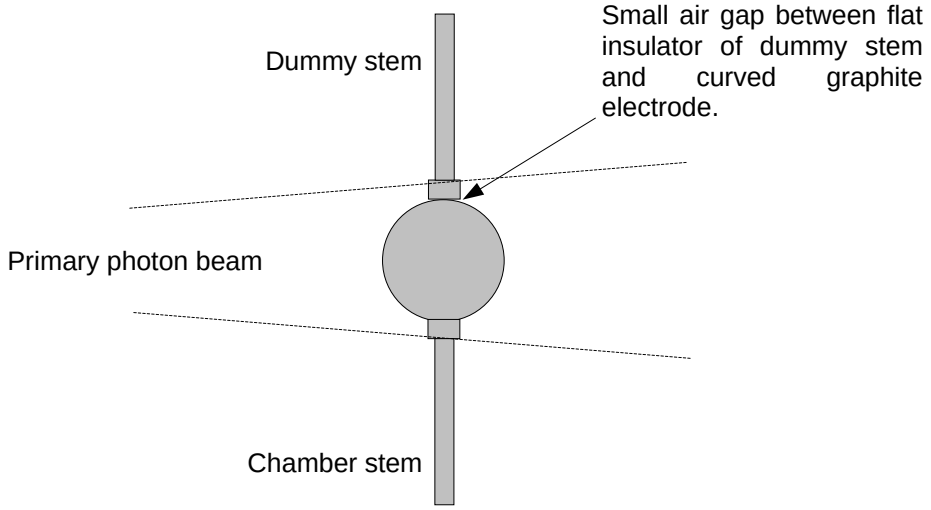

Figure 16. Experimental set-up for the determination of the stem scatter correction

The stem scatter correction is the ratio of the ionisation current measured without the dummy stem and the ionisation current measured with the dummy stem, both corrected for standard temperature and pressure and source decay. The ionisation current was measured without the dummy stem, then with the dummy stem and finally again without the dummy stem, i.e. the following measurement equation applies:

$$k_{stem} = \frac{\left(I^{(1)}_{chamber\_only} + I^{(2)}_{chamber\_only}\right)}{2 \cdot I_{with\_dummy\_stem}} \tag{3}$$

The stem scatter correction factor, k_{stem}, was determined three times and the mean value was found to be $k_{stem} = 0.9983$. The uncertainties will be discussed in section 4.1.5.

4.1.2 Ion recombination correction

When the cavity chamber is exposed to ionising radiation, due to the limited polarising voltage, some of the ions generated inside the air volume will recombine before reaching the collecting electrodes and therefore an ion recombination correction needs to be applied to the primary standard measurement. Recombination in ionisation chambers at therapy level dose rates is small but nevertheless significant for primary standard level dosimetry.

The various processes by which ions recombine in an ionisation chamber, initial recombination, back diffusion to the electrodes and volume recombination, have been reviewed by Boag (1987).

Initial recombination occurs when positive and negative ions formed in the same secondary electron path meet and recombine. It is independent of dose rate, since the number of tracks occurring per unit volume of air does not influence the recombination within a given track, unless the ion density becomes so great that the field strength is reduced, or the tracks begin to overlap. Diffusion loss is also independent of the dose rate. Both initial recombination and diffusion loss are proportional to the inverse of the polarising voltage.

Volume recombination occurs when ions produced in different tracks encounter each other as they are attracted to the two electrodes. The amount of volume recombination depends on the ion density and therefore on the dose rate and it is proportional to the inverse of the square of the polarising voltage (Attix 1986, Takata *et al.* 2005).

Numerous methods have been published to estimate the recombination correction in ionisation chambers. For the NPL primary standard cavity chamber the Niatel/Boutillon method (Boutillon 1998) was adopted to determine the recombination correction experimentally. This method applies to continuous radiation and allows separation of the contribution due to volume recombination from the combined contributions of initial recombination and diffusion losses. The cavity ionisation chamber was developed for the measurement of gamma radiation emitted by HDR ^{192}Ir brachytherapy sources, but since ion recombination is independent of beam quality for sparsely ionising radiation, the recombination measurements were performed, for convenience, using an X-ray set (Figure 17).

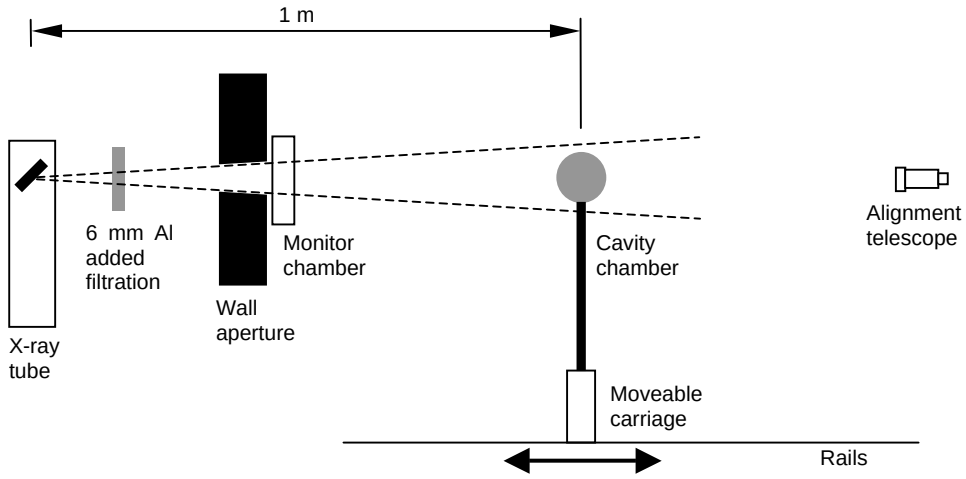

Figure 17. Set-up for ion recombination measurements, side view (not to scale)

The tube voltage was set to 50 kV and a 6 mm thick aluminium filter was added to reduce the dose rate. The cavity chamber was set up at a focal distance of 1 m and various tube currents were selected: 0.25 mA, 0.5 mA, 1 mA, 2 mA, 3 mA and 5 mA. This range of tube currents was chosen to provide dose rates similar to those normally generated by HDR ^{192}Ir brachytherapy sources with nominal initial activities in the order of 370 GBq when using the standard set-up for the measurement of RAKR shown in Figure 8 and 9. A transmission monitor chamber was used to normalise the measured ionisation currents for any drifts in the X-ray tube output.
Experimental methods to determine the correction for ion recombination are based on the assumption that if a sufficiently high polarising voltage is applied to the chamber, the ions would be collected before they had a chance to recombine, so long as the high field strength does not introduce some other effect such as ionisation by collision. The standard polarising voltage (500 V) for the cavity chamber was found by plotting the variation of the collected ionisation current as a function of the polarising voltage (Figure 18). 500 V is well on the plateau region of the saturation curve without any effect of charge multiplication yet occurring, as can be seen from Figure 19.

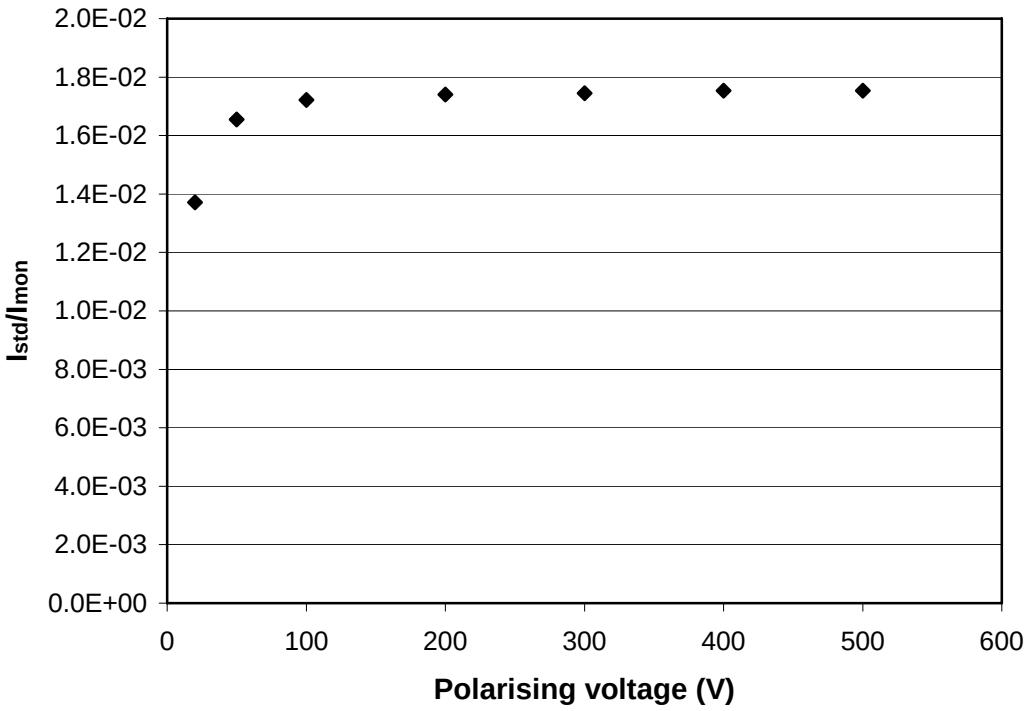

Figure 18. Variation of the collected ionisation current as a function of the polarising voltage (saturation curve)

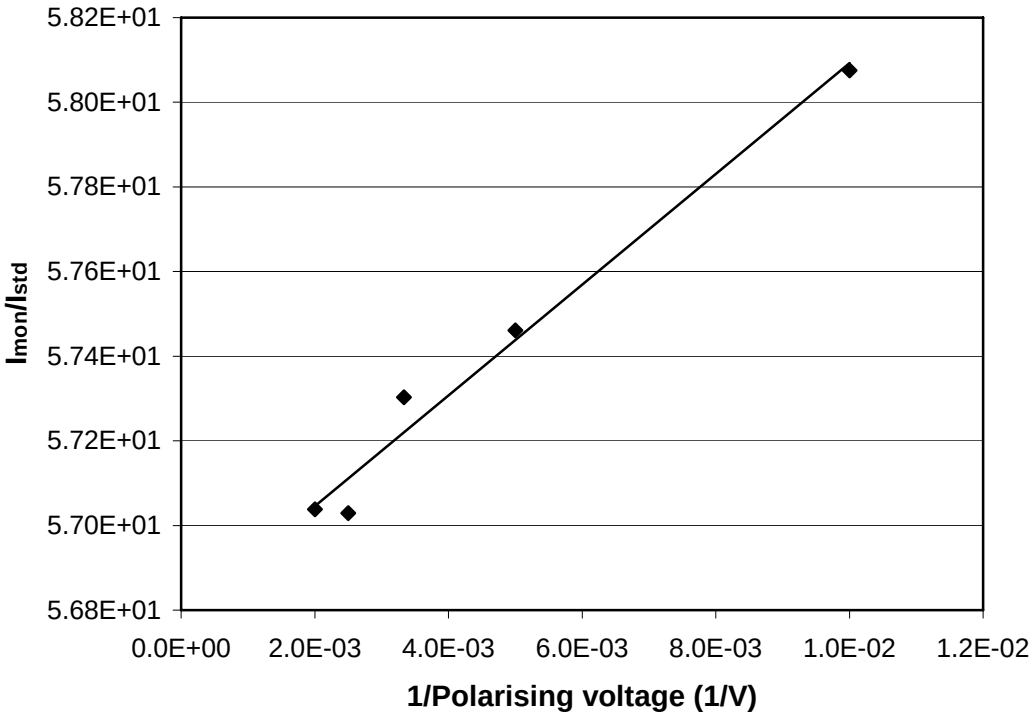

Figure 19. Inverse ionisation current *vs* inverse polarising voltage over the range V = 100 V to 500 V, where initial recombination dominates

Near saturation, the ratio between the saturation current I_S and the ionisation current I_V, measured at voltage V, can be expressed, neglecting terms of higher order, by the basic equation (Boutillon 1998)

$$\frac{I_S}{I_V} = 1 + \frac{A}{V} + m^2\left(\frac{g}{V^2}\right)I_S \tag{4}$$

where

$$m^2 = \frac{\alpha}{ek_+k_-} \tag{5}$$

and where A is a constant depending on the chamber type, α is the recombination coefficient under continuous irradiation, e is the electron charge, k_+ and k_- are the mobilities of the positive and negative ions, and g is a factor depending on the chamber geometry. The first variable term on the right hand side of Equation 4 describes the initial recombination and diffusion; the second variable term describes the volume recombination.

For the determination of the parameters A and m^2g, V in Equation 4 is replaced by the lower voltage V/n where n is not necessarily an integer, and the new equation obtained is divided by Equation 4 to give

$$\frac{I_V}{I_{V/n}} = 1 + \underbrace{\frac{(n-1)A}{V}}_{\text{intercept}} + \underbrace{(n^2-1)m^2\left(\frac{g}{V^2}\right)}_{\text{gradient}} I_V \quad . \tag{6}$$

(see Figure 20)

Equation 6 applies as long as I_V is close to the saturation current. High-order terms are neglected.

For each setting of tube voltage and tube current, the ionisation current was measured for selected polarising voltages V (here: 500 V, i.e. the standard operating voltage) and V/n (here: n = 2, 2.5, 3 and 3.5) and the ratio $I_V/I_{V/n}$ was plotted against I_V (Figure 20). Measurements of I_V and $I_{V/n}$ were made for both polarities and the mean was taken as the effective value. The settling time after each change in polarising voltage was at least 15 minutes and a pre-irradiation was given to eliminate any accumulated charge.

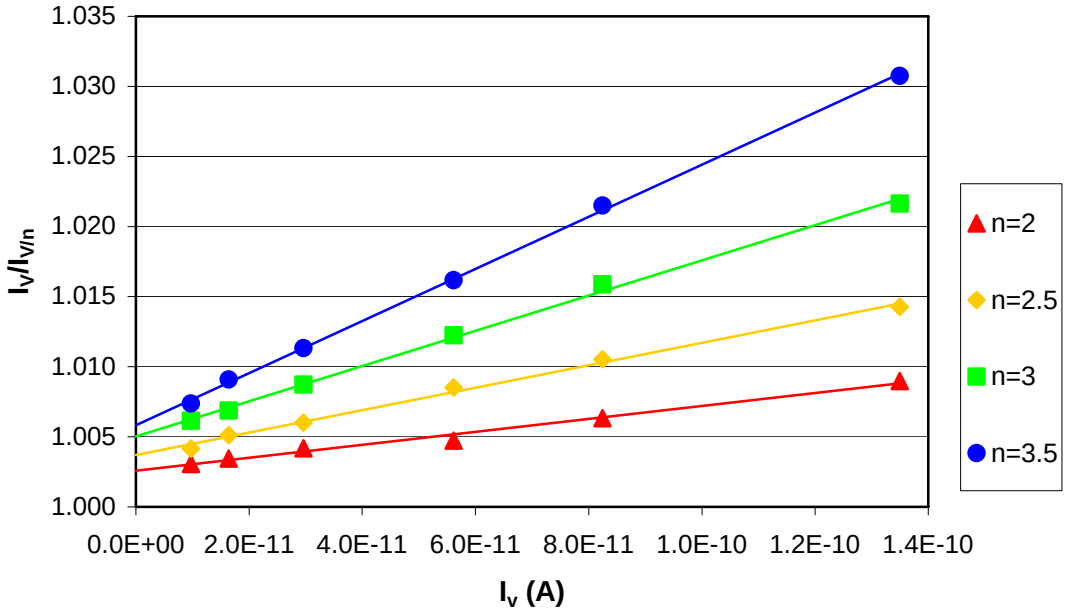

Figure 20. Ratio of the ionisation currents I_V and $I_{V/n}$, measured with chamber TH100C with polarising voltages V and V/n respectively, as a function of I_V, for several values of n

Four straight lines were fitted to the data points in Figure 20. The slopes and the intercepts of these lines were determined by regression analysis, allowing the determination of the factors A and m^2g in Equation 6. The results are summarised in Table 9.

Table 9. Summary of ion recombination measurements

n	Intercept	Slope	A	m^2g
2.0	1.0026	4.625×10^7	1.291	3.854×10^{12}
2.5	1.0037	8.007×10^7	1.237	3.813×10^{12}
3.0	1.0050	1.257×10^8	1.255	3.927×10^{12}
3.5	1.0058	1.859×10^8	1.167	4.131×10^{12}
		Mean value, $\bar{x}$	**1.238**	**3.931×10^{12}**
		$\sigma_{n-1}/\bar{x}$ (%)	4.2	3.6

Table 10 lists the total recombination correction factors $I_S/I_V = k_{ion}$ (see Equation 4) with respect to the measured ionisation current at the standard polarising voltage of 500 V.

Table 10. Recombination correction with respect to ionisation current

Initial recombination	Volume recombination	$I_S/I_V = k_{ion}$	$I_{V(=500V)}$ (pA)
2.48×10^{-3}	1.53×10^{-4}	1.0026	9.75
2.48×10^{-3}	2.58×10^{-4}	1.0027	16.40
2.48×10^{-3}	4.66×10^{-4}	1.0029	29.64
2.48×10^{-3}	8.83×10^{-4}	1.0034	56.15

The calculated recombination correction factors were plotted against the measured ionisation currents in pA (Figure21).

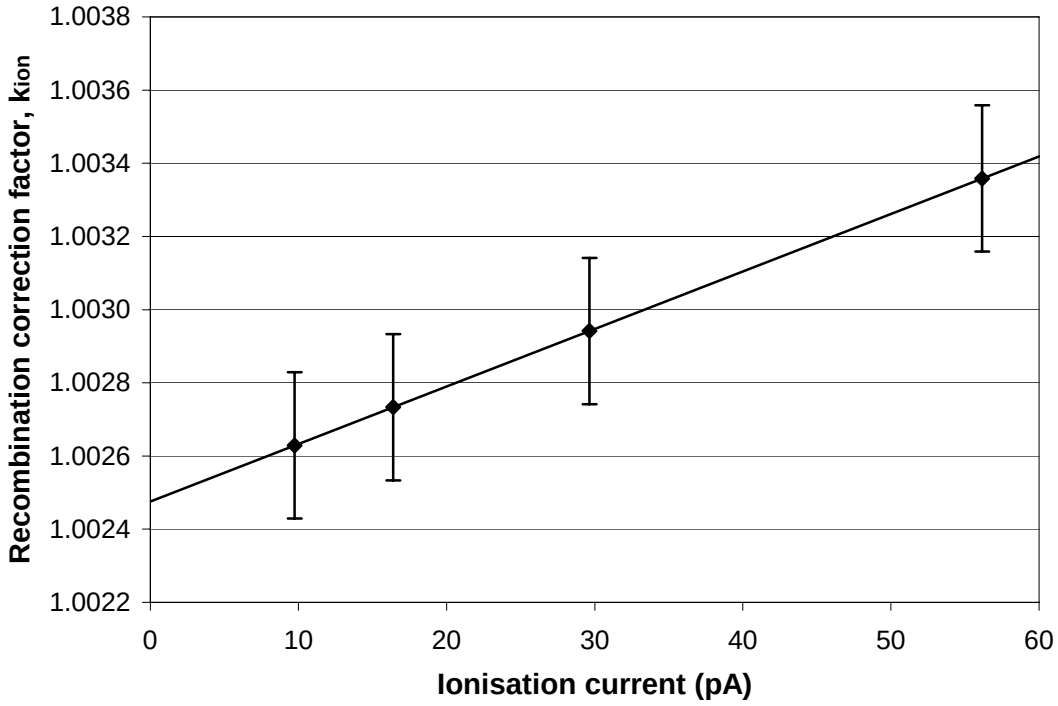

Figure 21. Recombination correction k_{ion} as a function of the ionisation current I_V

The recombination correction factor k_{ion} for the primary standard cavity chamber TH100C can be represented by the following equation

$$k_{ion} = (1.0025 \pm 0.0002) + ((1.57 \pm 0.09) \cdot 10^7) \cdot I_V \quad (7)$$

where I_V is the measured ionisation current in A. For the typical currents measured when a new brachytherapy source is installed, this results in a recombination correction factor of k_{ion} = 1.0028 ± 0.0002. The uncertainties in the initial and volume recombination will be discussed in section 4.1.5.

A new Nucletron microSelectron HDR ^{192}Ir source has a nominal initial activity of between 370 GBq and 550 GBq. This is equivalent to ionisation currents of 18.7 pA and 27.8 pA, respectively, measured with the primary standard chamber at an SCD of 1433 mm. Additionally, the source has a relatively short half-life and so the source activity will vary from one measurement to another. k_{ion}, which is dose rate dependent, needs to be determined for each primary standard measurement of the reference air kerma rate.

4.1.3 Polarity correction

All measurements are normally made with a positive voltage, +500 V, supplied to the central (collecting) electrode and the chamber stem (guard). The graphite sphere is earthed.

The polarity correction was determined by reversing the polarising voltage of the ionisation chamber and by measuring the ionisation current with both positive and negative polarity HT on the central collecting electrode with respect to the earthed graphite sphere. The negative ionisation currents collected with the collecting electrode at positive potential were found to be consistently higher and the polarity correction factor was estimated using the following equation

$$k_{pol} = \frac{I^+ + I^-}{2 \cdot I^+} \quad (8)$$

where I^+ is the ionisation current collected at the standard setting (collecting electrode at positive potential: +500 V) and I^- is the ionisation current collected with the collecting electrode at negative potential (-500 V). First, I^+ was measured, then I^- and finally I^+ again. The following measurement equation describes the measurement of the polarity correction factor:

$$k_{pol} = \frac{\frac{I^{+(1)} + I^{+(2)}}{2} + I^-}{2 \cdot \frac{I^{+(1)} + I^{+(2)}}{2}} = \frac{1}{2} + \frac{I^{(-)}}{I^{+(1)} + I^{+(2)}} \quad (9)$$

The polarity correction factor, k_{pol}, was determined four times and the mean value was found to be $k_{pol} = 0.9983$. The uncertainties will be discussed in section 4.1.5.

The results of these measurements (stem scatter, ion recombination and polarity correction) can be found in the folder labelled 'Brachytherapy primary standard TH100C – Measured chamber correction factors (October – December 2005)'.

4.1.4 Dead volume correction

In cylindrical cavity chambers, where two conducting surfaces meet at an angle of 90º, the effective collecting volume is smaller than the geometric volume of the cavity because the electric field strength in close proximity to the corners of the graphite cap is $\left|\vec{E}\right| \cong 0$. Charged particles generated in this region will therefore not contribute to the collected ionisation current and a dead volume correction greater than unity will have to be applied to the measured current.

Due to the spherical geometry of the cavity chamber TH100C and the absence of corners between conducting surfaces, there is no dead volume inside the air cavity. A simulation of the electric field between the central electrode and the earthed, spherical electrode was made using the proprietary software package COMSOL Multiphysics™ (2005). A 2D geometry with axial symmetry was chosen for the finite element analysis. Figure 22 shows the equipotential field lines between the central collecting electrode and the earthed graphite sphere. Due to the evenly distributed electric field the effective collecting volume was assumed to be identical with the geometric volume of the air cavity. The potential dead volume in the vicinity of the insulator was found to be negligible. No uncertainty was assigned to the dead volume correction.

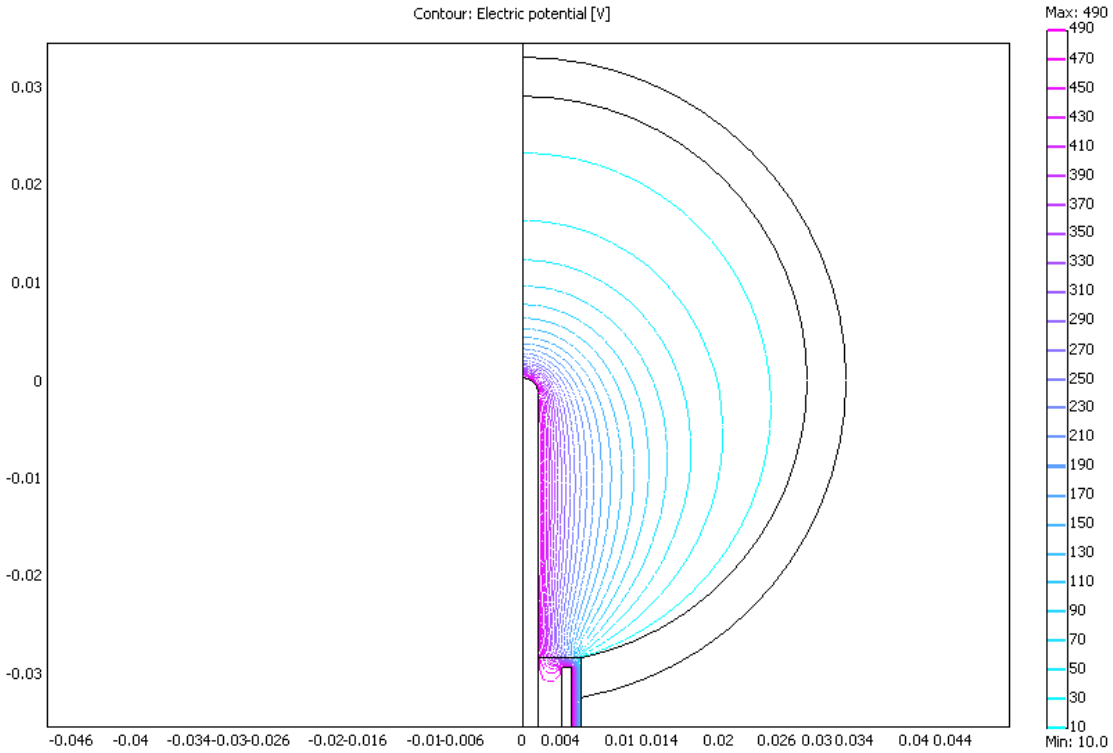

Figure 22. Equipotential field lines between the central electrode (+500 V) and the spherical electrode (earth) calculated using finite element analysis

4.1.5 Uncertainties in the measured correction factors

For the stem scatter correction factor, a type A uncertainty of 0.02% (k = 1) was derived from the standard deviation of the mean of three measurements. A type B uncertainty of 0.05% was assigned to the stem scatter correction factor due to the fact that the top of the dummy stem was not curved, leaving a small air gap between the graphite boss and the curved electrode, i.e. the dummy stem, although made of the same materials as the chamber stem and having the same dimensions, was not a perfect copy. Therefore, the dummy stem did not have the same scatter properties as the chamber stem. Summing the squares of the type A and B uncertainties and taking the square root gave an overall standard uncertainty in k_{stem} of 0.05%.

No type A uncertainty could be assigned to the initial and volume recombination correction factor because the relatively complex experimental determination of k_{ion} was only made once. The relative standard uncertainties (type B) in the intercepts and gradients of the lines plotted in Figure 20 were determined by regression analysis. The mean values for the constants A and $m^2 g$ (see Table 9) were inserted in Equation 4 and the type B uncertainties of the two terms representing the initial and volume recombination were calculated for a standard polarising voltage $V = 500\,\mathrm{V}$ and a maximum ionisation current of $I_S = 30\,\mathrm{pA}$. The maximum standard uncertainty in the intercept (equivalent to the initial recombination correction factor, see Equation 4 and 6) was 0.022%. The maximum standard uncertainty in the gradient was found to be 5.6%, which is equivalent to a standard uncertainty in the volume recombination correction of 0.003%, assuming an ionisation current of $I_S = 30\,\mathrm{pA}$. The combined standard uncertainty in k_{ion} was 0.02%.

For the polarity correction factor, a type A uncertainty of 0.01% (k = 1) was assigned which was the standard deviation of the mean of four correction factors. No type B uncertainty was assigned to the polarity correction factor.

4.2 Summary of the measured correction factors

Table 11. Uncertainties in the measured primary standard correction factors. All uncertainties are quoted for 2 standard deviations.

Factor		Mean values	Type A uncer-tainty (%)	Type B uncer-tainty (%)	Total uncer-tainty (%)
$k_{stem} = k_1$	Stem scatter correction	0.9983	0.04	-	0.04
$k_{ion} = k_2$	Ion recombination correction	1.0028*)	-	0.04	0.04
$k_{pol} = k_3$	Polarity correction	0.9983	0.02	-	0.02

*) typical value (for 20 pA ionisation current)

4.3 Overview of Monte Carlo simulations

Some of the primary standard correction factors were evaluated by calculation using Monte Carlo techniques. This section gives an overview of the Monte Carlo codes used.

4.3.1 The Monte Carlo Code Systems

The spectrum from the Nucletron HDR brachytherapy Classic source after collimation was determined using the OMEGA BEAM (EGS4) code system. All of the subsequent Monte Carlo calculations described in this report were carried out using the EGSnrc code system. These codes form a general-purpose package for the Monte Carlo simulation of the coupled transport of electrons and photons in an arbitrary geometry for particles with energies ranging from a few keV to several TeV (Kawrakow 2000). The EGSnrc package, used in conjunction with a user-written code, calculates the development of an electron-photon cascade from a single incident electron or photon, and transports each particle through the geometry until it reaches a predefined energy cut-off or discard boundary. The BEAM package is EGS4 code for modelling beams from a user specified module (Rogers *et al.* 1995). Electron-photon transport can be simulated in any of 100 chemical elements or mixture of these elements, or any compound. The associated package PEGS4, documented by Nelson *et al.* 1985, is used to generate datasets for particle transport and sampling of the required materials for subsequent use by BEAM and EGSnrc.

4.3.2 Description of the EGSnrc User Codes

The two EGSnrc user codes used in this work, CAVRZnrc and DOSPHEREnrc, are able to read in the phase space information generated by the OMEGA BEAM code system. CAVRZnrc calculates the dose deposited to user-specified regions of an RZ geometry. DOSPHEREnrc calculates the dose deposited to the user-specified regions of a spherical geometry made up of concentric spheres of varying radii, enclosed within an XYZ geometry. Both codes have undergone a series of benchmark tests checking energy conservation and uncertainty analysis.

4.3.3 PEGS4 Data sets

Within the PEGS4 input files the values of AE and AP were set to 0.516 MeV and 0.001 MeV for all materials. The IAPRIM (Rogers *et al.* 1989) and EPSTFL (Duane *et al.* 1989) options that are set within the PEGS4 input files were used. The IAPRIM option normalises the bremsstrahlung cross-sections so that PEGS4 gives the same radiative stopping power for electrons as given in ICRU Report 37 (ICRU 1984). The EPSTFL option allows the user to input an arbitrary density-effect correction for use in calculating electron and positron collision stopping powers. The density effect corrections were obtained using the program EPSTAR[(2)] (S. M. Seltzer - version 2.0B) and these values were then used in conjunction with the PEGS4 input files to create the material data sets.

For the simulations calculating the response of the air equivalent chamber the materials specified used the density effect corrections for normal density air and for

[(2)] Calculates stopping power (collisional, radiative and total), CSDA ranges, bremsstrahlung yield for electrons (or positrons) with kinetic energies from l keV to 10 GeV and the mean excitation energy of the material

the simulations calculating the response of the graphite equivalent chamber the materials specified used the density effect corrections for normal density graphite.

4.3.4 Calculation of the shielded ^{192}Ir spectrum from a Nucletron Classic source

The 11 major lines contributing to the ^{192}Ir spectrum were used as input to the BEAM simulation (Loftus 1980). Due to limitations with the geometry packages available with BEAM the source design was approximated to a cylindrical geometry without shielding modelled at either ends of the source. It was shown that the lack of shielding made no difference to the calculated spectrum. Both of these approximations were considered to be adequate as simulations carried out using the average ^{192}Ir energy instead of a calculated spectrum gave a change to the overall calculated correction factor of the order 0.1%. The front face of the lead collimator was included in the simulation model and the spectrum stored at a pre-defined scoring plane for use in subsequent Monte Carlo simulations.

4.4 Correction factors determined by Monte Carlo simulation

4.4.1 Overview

The HDR brachytherapy primary standard cavity chamber collects charged particles which are produced by photons scattering in the graphite wall. Compton electrons produced in the chamber wall enter the air cavity. However, the chamber wall attenuates the incident photons, scattered photons produce a response and the chamber material near the cavity is not air-equivalent. It is also possible for a photon to scatter twice and the knock on electron from the second scatter to contribute to ionisation.

The air kerma in air is given by the following:

$$K_a = \frac{Q}{m} \cdot \frac{W}{e} \cdot \frac{F}{(1-g)} \tag{10}$$

where Q is the measured charge,
m is a known mass of air,
W is the energy needed to create an ion pair in dry air,
e is the electron charge,
g is the fraction of energy lost to bremsstrahlung

and
$$F = \widetilde{F} \cdot k_{an} \cdot k_{rn} \cdot k_{stem} \cdot k_{pol} \cdot k_{ion} \tag{11}$$

where k_{an} is the axial non-uniformity correction,
k_{rn} is the radial non-uniformity correction,
k_{stem} is the stem scatter correction,
k_{pol} is the polarity correction,
k_{ion} is the ion recombination correction,

and $$\widetilde{F} = \overline{S}_{air}^{graphite} \cdot k_{fl} \cdot (\overline{\mu}_{en}/\rho)_{graphite}^{air} \cdot k_{wall} \quad (12)$$

where $\overline{S}_{air}^{graphite}$ is the ratio of the mean stopping powers of graphite and air,

k_{fl} is the fluence perturbation correction, correcting for the perturbation of the electron fluence by the air cavity,

$(\overline{\mu}_{en}/\rho)_{graphite}^{air}$ is the ratio of the mean mass-energy absorption coefficients of air and graphite and

k_{wall} is the wall correction factor.

$\widetilde{F}$ is the ratio of the dose to the chamber volume in the absence of the chamber, and what is actually measured, the chamber response. Monte Carlo simulations carried out using DOSPHEREnrc were used to determine this ratio:

$$\widetilde{F} = \frac{D_{cav,air}\,(\text{no attenuation, no scatter})}{D_{cav,real}\,(\text{total}) \cdot k_{cel}} \quad (13)$$

where $D_{cav,air}(\text{no attenuation, no scatter})$ is the dose to the cavity of an air equivalent chamber (see Figure 24) where incident photons that interact in the chamber wall are not attenuated and the scattered photon is discarded; $D_{cav,real}(\text{total})$ is the total dose to the air cavity of the actual chamber (without central electrode) with real materials modelled (see Figure 24); k_{cel} is the correction to account for the effect of the graphite central electrode.

$\widetilde{F}$ can be divided into it's component parts by taking ratios of calculated doses:

$$\frac{D_{cav,air}\,(\text{no attenuation, no scatter})}{D_{cav,graphite}\,(\text{no attenuation, no scatter})} = \frac{\int_0^{E_0} dE \cdot \psi_\gamma(E) \cdot (\mu_{en}(E)/\rho)_{air}}{\int_0^{E_0} dE \cdot \psi_\gamma(E) \cdot (\mu_{en}(E)/\rho)_{graphite}} = (\overline{\mu}_{en}/\rho)_{graphite}^{air} \quad (14)$$

where $D_{cav,graphite}(\text{no attenuation, no scatter})$ is the dose to the cavity of a graphite equivalent chamber where incident photons that interact in the chamber wall are not attenuated and the scattered photon is discarded and $\psi_\gamma(E)$ is the photon energy fluence crossing the cavity.

$$\frac{D_{cav,graphite}\,(\text{no attenuation, no scatter})}{D_{cav,real}\,(\text{no attenuation, no scatter})} = \frac{\int_0^{E_0} dE \cdot \phi_{e^-}(E) \cdot S_{graphite}}{\int_0^{E_0} dE \cdot \phi_{e^-}(E) \cdot S_{air}} \cdot k_{fl} = \overline{S}_{air}^{graphite} \cdot k_{fl} \quad (15)$$

where $D_{cav,real}(\text{no attenuation, no scatter})$ is the dose to the air cavity of the actual chamber with real materials modelled where the incident photons that interact in the

chamber wall are not attenuated and the scattered photon is discarded and $\phi_{e^-}(E)$ is the electron energy fluence crossing the cavity.

$$\frac{D_{cav,real}(\text{no attenuation, no scatter})}{D_{cav,real}(\text{total}) \cdot k_{cel}} = k_{wall} \tag{16}$$

where k_{wall} is the wall correction and can be expressed as $k_{wall} = \beta_{cep}^{-1} \cdot k_{att} \cdot k_{scat}$

where β_{cep}^{-1} is a correction to account for a change in the centre of electron production

k_{att} is the wall attenuation correction

k_{scat} is the wall scatter correction

These components are calculated using the following equations:

$$\frac{D_{cav,real}(\text{no attenuation, no scatter})}{D_{cav,real}(\text{with attenuation, no scatter})} = \beta_{cep}^{-1} \cdot k_{att} \tag{17}$$

$D_{cav,real}(\text{with attenuation, no scatter})$ is the dose to the air cavity of the actual chamber with real materials modelled where the incident photons that interact in the chamber wall are attenuated and the scattered photon is discarded.

$$\frac{D_{cav,real}(\text{with attenuation, no scatter})}{D_{cav,real}(\text{ total}) \cdot k_{cel}} = k_{scat} \tag{18}$$

There is a further axial non-uniformity correction, k_{an}, required to account for the change in the spectrum over the chamber volume in the direction of the beam axis and a radial non-uniformity correction, k_{rn}, required to account for the change in the spectrum over the chamber volume perpendicular to the beam axis.

$$\frac{K_a}{D_{cav,air}(\text{no attenuation, no scatter})} = k_{an} \cdot k_{rn} \tag{19}$$

Further simulations were carried out using CAVRZnrc to determine the effect of the air gap between the 2 hemispheres making up the spherical chamber and the graphite central electrode, k_{cel}, see Figure 1. For these simulations similar dimensions were used but for a cylindrical chamber and the air gap was approximated with a simple straight through air gap of the maximum dimension measured. It was found to have a negligible effect on the correction factor. k_{cel} was similarly determined using simulations modelling with and without a cylindrical central electrode and ratios of total doses taken.

k_{an} was determined by calculating K_a over the cross-sectional area of the chamber. This was determined by modelling a thin cylindrical slab of air of the same size cross-section as the chamber volume using CAVRZnrc (with no electron transport). In order to determine k_{rn} the photon energy fluence was binned over the chamber volume and compared to the photon energy fluence at the centre of the chamber. k_{rn} was found to be negligible.

$(1-g)^{-1}$ was determined by repeating Monte Carlo simulations of the air equivalent chamber with bremsstrahlung switched off and taking ratios with and without

bremsstrahlung production. This Monte Carlo calculated factor showed good agreement with tabulated values (Boutillon and Perroche 1985).

The material correction factor $k_{material}$ for the cavity chamber was estimated to be unity since the surface area of the insulator between the central electrode and the spherical graphite wall is only 1% of the surface area of the graphite facing the air cavity. The insulators used in the chamber stem are graphite equivalent.

4.4.2 Simulation geometry

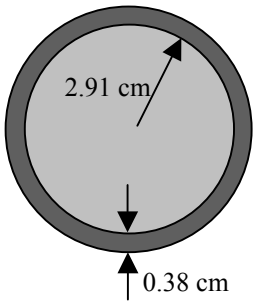

Figure 23: Simulation geometry - real chamber

Air of density 1.205E-3 g/cm^3

Graphite of density 1.75 g/cm^3

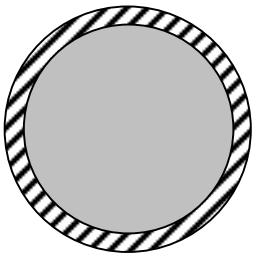

Figure 24: Simulation geometry - air equivalent chamber

Air of density 1.205E-3 g/cm^3

Air of density 1.75 g/cm^3

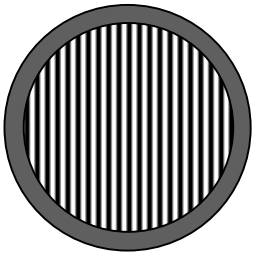

Figure 25: Simulation geometry - graphite equivalent chamber

Graphite of density 1.205E-3 g/cm^3

Graphite of density 1.75 g/cm^3

4.4.3 Uncertainties in the calculated correction factors

Estimates for the type A uncertainties in $\overline{S}_{air}^{graphite} \cdot k_{fl}$ and $(\mu_{en}/\rho)_{graphite}^{air}$ were obtained from determining the standard deviation on a total of six independent calculations of these factors. These calculations were made for three chambers with the same internal radius but with slightly varying wall thicknesses varying from 3.6 mm to 4.0 mm (reflecting the worst-case variation in the measured wall thickness) at 2 different source-chamber distances (1 m and 1.433 m). It was shown that these factors were independent of source-chamber distance and, to some extent, wall thickness and so the type A uncertainties could be reduced by a factor $\sqrt{N}$ where N was the number of independent determinations of the factor. The type A uncertainty in k_{wall} was assumed to be the same as for $\overline{S}_{air}^{graphite} \cdot k_{fl}$ and $(\mu_{en}/\rho)_{graphite}^{air}$ as the uncertainties determined in

the Monte Carlo simulations were very similar for all chamber geometries modelled for this work. There was also a small additional uncertainty associated with k_{cel}, however, this was negligible due to the size of the correction.

An estimate for the type B uncertainty in $\overline{S}_{air}^{graphite} \cdot k_{fl}$ was determined by calculating a worst-case set of stopping power values for each material and taking an average of the ratio for the shielded ^{192}Ir spectrum and comparing with standard data. The value of this uncertainty was very similar to that taken from Rapport BIPM-99/12, Comparison of the air kerma standards of the NRC and the BIPM for ^{60}Co gamma rays. This report quotes a reduced uncertainty in the stopping power ratio when combined with W/e. An estimate for the type B uncertainty in $(\mu_{en}/\rho)_{graphite}^{air}$ was also taken from this report. Both estimates used were the same as those for the NRC graphite-walled cylindrical cavity ionisation chamber. The type B uncertainty in k_{wall} was based on the calculated change in the factor (0.2%) with a change in wall thickness of 0.2 mm combined with the uncertainty in not applying a correction for the effect of the air gap. The type A and B uncertainties in k_{cel} were determined previously from Monte Carlo simulations.

The type A uncertainty in k_{an} was estimated to be the same as for the other Monte-Carlo calculated factors for the same reasons as discussed previously. The type B uncertainty in k_{an} is estimated to be the size of the correction.

The estimate for the type A uncertainty in k_{rn} was estimated by comparing values determined using different binning techniques. The type B uncertainty in k_{rn} is the maximum deviation from unity determined.

Estimates for the type A and type B uncertainties in $(1-g)^{-1}$ were taken from Rogers *et al.* (1989).

The shielded ^{192}Ir spectrum was determined using only the 11 major contributing lines as input to the OMEGA BEAM simulation. The effect of neglecting less significant lines was considered negligible as the effect to the overall correction factor of using the average ^{192}Ir energy as input to the EGSnrc simulations instead of a calculated spectrum was determined to be of the order 0.1%.

4.5 Summary of all calculated correction factors

Table 12. Uncertainties in the stopping power ratio (graphite to air), the mass energy absorption coefficient ratio (air to graphite) and all calculated primary standard correction factors

Factor		Mean values	Type A uncer-tainty (%)	Type B uncer-tainty (%)	Total uncer-tainty (%)
$\overline{S}_{air}^{graphite} \cdot k_{fl}$	Stopping power ratio (graphite to air) x fluence perturbation correction	1.0082	0.1	0.23[(1)]	0.25
$(\overline{\mu}_{en}/\rho)_{graphite}^{air}$	Mass energy absorption coefficient ratio (air to graphite)	1.0016	0.1	0.2	0.22
$\beta_{cep}^{-1} \cdot k_{att}$	Wall attenuation correction	1.1229	-	-	-
k_{scat}	Wall scatter correction	0.9309	-	-	-
$k_{wall} = \beta_{cep}^{-1} \cdot k_{att} \cdot k_{scat} = k_4$	Wall correction	1.0453	0.1	0.23	0.25
$k_{cel} = k_5$	Central electrode correction	0.9984	0.1	0.05	0.11
$\widetilde{F} = \overline{S}_{air}^{graphite} \cdot k_{fl} \cdot (\mu_{en}/\rho)_{graphite}^{air} \cdot k_{wall}$		1.0555	0.17	0.38	0.42
$k_{an} = k_6$	Axial non-uniformity correction	0.9981	0.1	0.2	0.22
$k_{rn} = k_7$	Radial non-uniformity correction	1.0000	0.01	0.04	0.04
$(1-g)^{-1}$	Fraction of energy lost by bremsstrahlung	1.0007	0.02	0.02	0.03

(1) Combined uncertainty for the product $\left(\overline{S}_{air}^{graphite} \cdot W/e\right) \cdot k_{fl}$

5 Air attenuation and scatter correction

An air attenuation and scatter correction needs to be applied to measurements of the RAKR due to the fact that the measurements are made in air and not in free space (see definition of RAKR; ICRU 1985 and 1997). k_{aa} is the correction for attenuation of the primary photons by the air molecules between the source and the chamber. k_{sc} is the correction for scattered radiation from the floor, walls, measurement set-up and air. Both k_{aa} and k_{sc} are proportional to the number of air molecules between the source and the ionisation chamber. The total air attenuation and scatter correction, k_{air}, was determined by applying a multiple distance method. The primary standard

cavity chamber was set up on the central beam axis and moved to various positions along the rails (see Figure 8 and 9). The ^{192}Ir source was aligned on the central beam axis of the lead collimator. A pre-measurement dose was delivered to the chamber to eliminate any charge that may have built up on the insulator while the chamber was not in use. The leakage current from the cavity chamber was found to be negligible, i.e. less than 0.1% of the measured current. Readings of the ionisation current were taken at centre-to-centre source-chamber distances between 1.233 m and 4.033 m at 0.2 m intervals and all current readings were normalised to the reference distance of 1 m by applying the inverse square law. During each measurement, readings of the temperature and pressure were recorded which allowed the measurements to be corrected to standard temperature ($T_0 = 293.15$ K) and pressure ($p_0 = 101.325$ kPa). The time at which each measurement was made was also recorded so that a decay correction could be applied to a reference time and date. The ionisation current at the reference time, for standard atmospheric conditions and normalised to the reference distance of 1 m, is given by:

$$I_{ref} = I_{raw} \cdot k_{elec} \cdot \left(\frac{d}{d_{ref}} \right)^2 \cdot \frac{T}{T_0} \cdot \frac{p_0}{p} \cdot \exp\left(\frac{\ln 2 \cdot \left(t_{now} - t_{ref} \right)}{\tau_{1/2}} \right) \tag{20}$$

where I_{ref} is the normalised ionisation current in A, I_{raw} is the ionisation current displayed on the electrometer in A, k_{elec} is the electrometer correction factor, d is the measured centre-to-centre source-chamber distance in m, d_{ref} is the reference distance (1 m), T is the air temperature in K, T_0 is the standard temperature in K, p is the air pressure in kPa, p_0 is the standard pressure in kPa, t_{now} is the actual measurement time, t_{ref} is the reference time and $\tau_{1/2}$ is the half-life of ^{192}Ir in days.

Figure 26 shows the normalised ionisation current I_{ref} at nominal source to chamber distances. The linear plots show a decrease in the normalised ionisation current with increasing source to chamber distance. The increasing air absorption and air scatter out of the beam that would give a lower ionisation current within the chamber with increasing distance can explain this.

The nominal length of the air column between the source and the chamber was calculated by applying a temperature and pressure correction:

$$d_{nom} = d_{measured} \cdot \frac{T_0}{T} \cdot \frac{p}{p_0} \tag{21}$$

where d_{nom} is the nominal length of the air column between the source and the centre of the chamber, normalised to T_0 and p_0. $d_{measured}$ is the measured centre-to-centre source-chamber distance minus the wall thickness of the ionisation chamber, i.e. $d_{measured}$ is the length of the air column. The radius of the cylindrical source capsule is only 0.55 mm which is negligible compared to the measurement distance and has not been taken into account in this calculation. T_0, T, p_0 and p are the temperatures and pressures as defined for Equation 20. The nominal length is the length of the air column between the source and the chamber containing the same number of air

molecules (air attenuation and scatter centres) if the measurements made at T and p would have been carried out at T_0 and p_0.

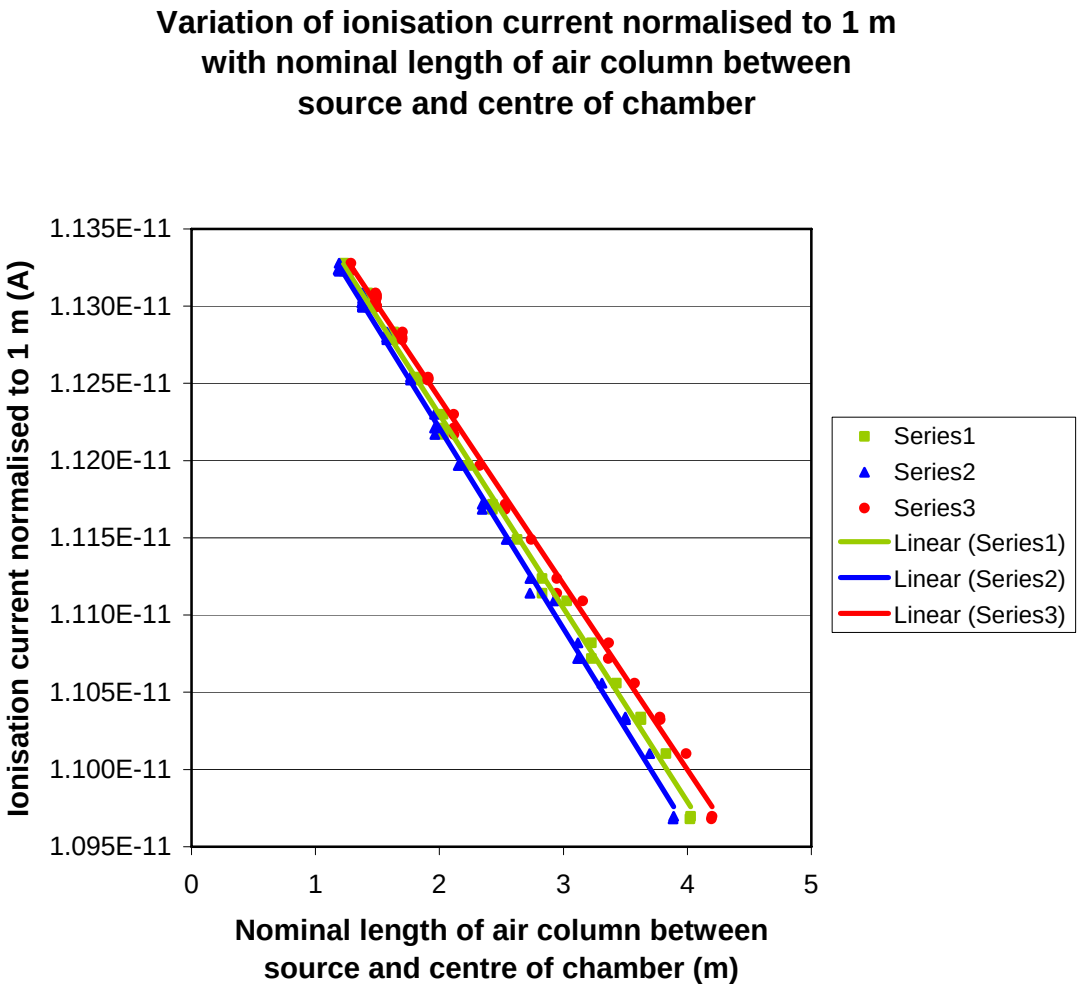

Figure 26. Variation of ionisation current normalised to 1 m with nominal length of air column between source and centre of chamber

Figure 26 shows the corrected ionisation currents normalised to 1 m, plotted against nominal source to chamber distances. The measured lengths (see Equation 21) were normalised to the following temperatures and pressures:

Series 1: T_0 = 293.15 K, p_0 = 101.325 kPa (standard atmospheric condition),

Series 2: $T_{0,2}$ = 290.65 K, $p_{0.2}$ = 104.000 kPa and

Series 3: $T_{0,3}$ = 295.65 K, $p_{0,3}$ = 98.000 kPa.

Series 1 is for air at standard temperature and pressure; series 2 and series 3 represent two extreme situations which could be experienced in the measurement room. Higher or lower temperatures and pressures are extremely unlikely.

Three lines were fitted to the measurement points of the three data series and the intercepts at 0 m (equivalent to the source centre) were determined. From Figure 26 it can be seen that the correction, which needs to be applied to the ionisation current to account for air attenuation and scatter, must be greater than unity. The air attenuation and scatter correction is the ratio of the normalised ionisation currents at 0 m (source

centre) and 1.429 m (centre-to-centre source-chamber distance minus thickness of graphite cap) and the correction is obtained through the relation:

$$k_{air} = \frac{I\,(0\,\mathrm{m})}{I\,(1.429\,\mathrm{m})} \quad . \tag{22}$$

Table 13 lists the normalised ionisation currents at 0 m (source centre) and 1.429 m and the air attenuation and scatter corrections for standard temperature and pressure and for two extreme conditions (high temperature, low pressure and low temperature, high pressure).

Table 13. Air attenuation and scatter correction for selected atmospheric conditions

Temperature (K)	Pressure (kPa)	Normalised ionisation current at 0 m (pA)	Normalised ionisation current at 1.429 m (pA)	Air attenuation and scatter correction, k_{air} (%)
295.65	98.000	11.480	11.308	1.52
293.15	101.325	11.480	11.301	1.58
290.65	104.000	11.480	11.295	1.64

A general expression for the calculation of the air attenuation and scatter correction was derived from Figure 27. Only two of the lines plotted in Figure 26 are considered for the derivation of the general equation, however, Equation 23 to 30 (see next page) will also apply to other conditions where $T \neq T_0$ and $p \neq p_0$.

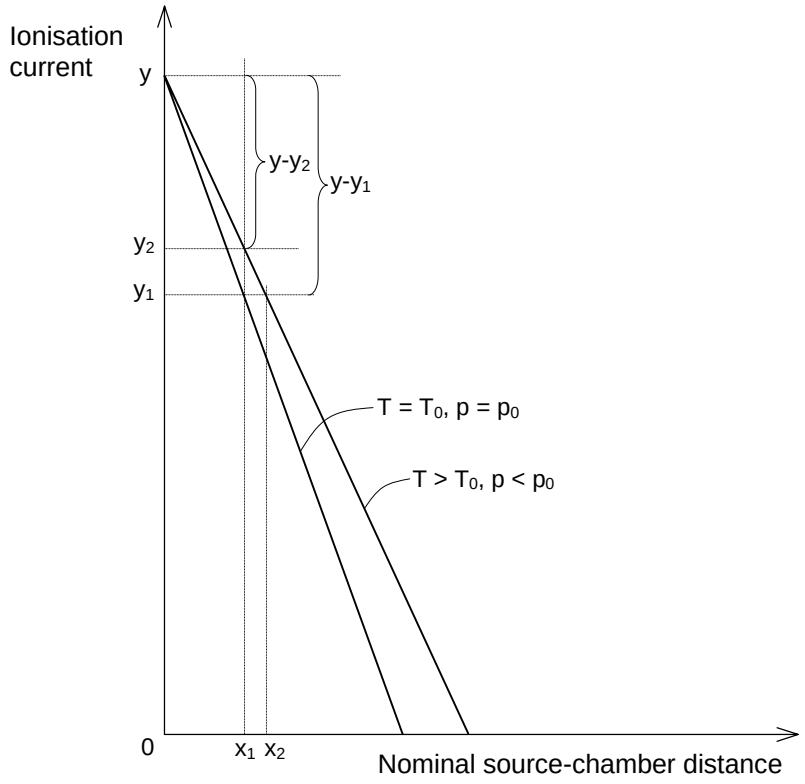

Figure 27. Symbols used for the derivation of a general expression for k_{air}

Let $x_1 =$ standard centre-to-centre source-chamber distance minus thickness of graphite cap (here: 1.429 m), $x_2 =$ length of air column x_1 normalised to $T > T_0$ and $p < p_0$, $y =$ normalised ionisation current at $x = 0$, $y_1 =$ normalised ionisation current at x_1 for STP and $y_2 =$ normalised ionisation current at x_1 for $T > T_0$ and $p < p_0$.

x_2 can be expressed as

$$x_2 = x_1 \cdot k_{TP} \tag{23}$$

where $k_{TP} = \frac{T}{T_0} \cdot \frac{p_0}{p}$ (temperature and pressure correction).
From the intercept theorem follows

$$\frac{x_2}{y - y_1} = \frac{x_1}{y - y_2} \tag{24}$$

and combining (23) and (24) gives

$$\frac{x_1 \cdot k_{TP}}{y - y_1} = \frac{x_1}{y - y_2} \tag{25}$$

or

$$1 = \frac{y - y_1}{y - y_2} \cdot k_{TP}^{-1} \ . \tag{26}$$

If the air temperature and pressure are slightly different from STP, the air attenuation correction at the nominal distance of 1.429 m varies only by a fraction of one per cent (see Table 13 for two extreme conditions) and $y_1 \cong y_2$ (1st order approximation). Equation (26) can therefore be approximated by

$$1 = \frac{y - y_1}{y - y_2} \cdot k_{TP}^{-1} \cong \frac{y_1}{y_2} \tag{27}$$

$$\frac{y - y_1}{y_1} \cdot k_{TP}^{-1} \cong \frac{y - y_2}{y_2} \tag{28}$$

$$\left(\frac{y}{y_1} - 1 \right) \cdot k_{TP}^{-1} \cong \left(\frac{y}{y_2} - 1 \right) \tag{29}$$

where $\left(\frac{y}{y_2}-1\right)$ is the air attenuation correction in % at distance x_1 for temperature T and pressure p, where y is the normalised current at $x=0\,\text{m}$ and y_2 is the normalised current at $x_1=1.429\,\text{m}$.

The combined air attenuation and scatter correction factor at $x_1=1.429\,\text{m}$, equivalent to a measured centre-to-centre source-chamber distance of 1.433 m, can be estimated by

$$k_{air}=1+\left(0.0158\cdot\frac{293.15}{T}\cdot\frac{p}{101.325}\right) \tag{30}$$

where T is the air temperature in K and p is the air pressure in kPa.

The standard uncertainty in k_{air} was found through regression analysis of the line fitted to data series 1 in Figure 26 (measurements made at standard temperature and pressure). The intercept was found to be $b=1.1480\text{E}-11$ with a standard uncertainty of 0.02% and the slope was found to be $m=-1.2534\text{E}-13$ with a standard uncertainty of 0.71%. The sensitivity coefficient for b was found to be 0.55 and the sensitivity coefficient for m was found to be 0.02.

The combined standard uncertainty of k_{air} was calculated as $u(k_{air})=\sqrt{(0.02\cdot 0.71\%)^2+(0.55\cdot 0.02\%)^2}=0.02\%$. The additional uncertainty due to the uncertainties in T and p (see equation 30) was found to be negligible.

6 Measurement equation

The NPL primary standard for the measurement of RAKR of HDR ^{192}Ir sources is a graphite-walled cavity ionisation chamber, based on Bragg-Gray cavity theory which relates the ionisation per unit mass in a small gas cavity to the energy absorbed per unit mass in the surrounding medium:

$$D_m=J_g W_g\frac{\overline{(S/\rho)_m}}{\overline{(S/\rho)_g}} \tag{31}$$

where D_m is the absorbed dose in the medium surrounding the cavity, J_g is the ionisation per unit mass in the cavity, W_g is the mean energy expended in the gas to produce an ion pair, and $\frac{\overline{(S/\rho)_m}}{\overline{(S/\rho)_g}}\equiv\left(\frac{\overline{S}}{\rho}\right)_g^m$ is the ratio of the mean electron-fluence-weighted electron mass stopping power of the medium to that of the gas (Seltzer and Bergstrom 2003). This relation is valid provided that the medium surrounding the cavity (here: graphite) is thick enough to exclude secondary electrons generated outside the chamber from entering the cavity, and that the cavity is small enough so as not to perturb the secondary electron fluence.

The absorbed dose in the gas (air), in the absence of the graphite wall is

$$D_g = D_m \frac{\overline{(\mu_{en}/\rho)_g}}{\overline{(\mu_{en}/\rho)_m}} \tag{32}$$

where $\frac{\overline{(\mu_{en}/\rho)_g}}{\overline{(\mu_{en}/\rho)_m}} \equiv \left(\overline{\frac{\mu_{en}}{\rho}}\right)_m^g$ is the ratio of the mean photon-energy-fluence-weighted photon mass energy-absorption coefficient of the gas to that of the graphite wall.

For graphite as the wall material and air as the cavity gas, the following measurement equation applies to the NPL brachytherapy primary standard cavity chamber and shows how the RAKR of an HDR ^{192}Ir source is determined from the measured ionisation current:

$$\dot{K}_R = \frac{\left(I_{raw} - I_{leakage}\right)\cdot k_{elec}}{\rho_{air}\cdot V_{air}} \cdot \frac{W_{air}}{e} \cdot \frac{1}{(1-\bar{g})} \cdot \left(\frac{\bar{S}}{\rho}\right)_{air}^{graphite} \cdot k_{fl} \cdot \left(\overline{\frac{\mu_{en}}{\rho}}\right)_{graphite}^{air} \cdot k_h \cdot \prod_i k_i \cdot \left(\frac{d}{d_{ref}}\right)^2 \cdot k_{air} \cdot k_{dec} \cdot k_{TP} \tag{33}$$

with the decay correction

$$k_{dec} = \exp\left(\frac{\ln 2 \cdot \left(t_{now} - t_{ref}\right)}{\tau_{1/2}}\right) \tag{34}$$

and the temperature and pressure correction

$$k_{TP} = \frac{T}{293.15} \cdot \frac{101.325}{p} \tag{35}$$

where

$\dot{K}_R$ is the reference air kerma rate (Gy/s) at the chosen reference time, t_{ref},

I_{raw} is the displayed ionisation current (A) on the electrometer,

$I_{leakage}$ is the leakage current (A),

k_{elec} is the electrometer correction factor,

ρ_{air} = 1.2045 kg/m^3 is the density of dry air (Davis 1992),

V_{air} = 1.02519E-4 m^3 is the cavity volume (see section 2.2.6) and

W_{air} is the average energy (J) spent by an electron of charge e (C) to produce an ion pair in dry air, where W_{air}/e = (33.97 ± 0.05) J/C (Boutillon and Perroche-Roux 1987). The uncertainty is given in the form of one standard deviation.

$\bar{g}$ = 0.0007 is the fraction of secondary electron energy lost to bremsstrahlung in air,

$\left(\frac{\bar{S}}{\rho}\right)_{air}^{graphite} \cdot k_{fl}$ = 1.0082 is the product of the ratio of the mean electron-fluence-weighted electron mass stopping power of graphite to that of air and the fluence perturbation correction factor,

$\left(\overline{\frac{\mu_{en}}{\rho}}\right)_{graphite}^{air}$ = 1.0016 is the ratio of the mean photon-energy-fluence-weighted photon mass energy-absorption coefficient of air to that of graphite,

k_h = 0.9970 is the humidity correction factor (Rogers and Ross 1988),

$\prod_i k_i$ is the product of all correction factors (i = 1, 2, 3,…, 7) to be applied to the primary standard (see Table 11 and 12),

$\left(\frac{d}{d_{ref}}\right)^2$ normalises the current measured at centre-to-centre source-chamber distance d = 1.433 m (see Figure 8 and 9) to the reference distance d_{ref} = 1 m (inverse square law),

k_{air} is the combined air attenuation and scatter correction which corrects the measured current at d = 1.433 m for air attenuation and scatter due to the air molecules between the source and the point of measurement (see Equation 30),

k_{dec} is the decay correction where

t_{now} is the actual measurement time,

t_{ref} is the reference time and

$\tau_{1/2}$ is the half-life of ^{192}Ir (73.827 days ± 0.013 days (DDEP 2005)).

If t_{ref} is before t_{now}, $\Delta t = t_{now} - t_{ref}$ is positive; if t_{ref} is after t_{now}, $\Delta t = t_{now} - t_{ref}$ is negative.

NB When secondary standard ionisation chambers are calibrated with the calibrated source, the ionisation current must be corrected to the same reference time, t_{ref}, before the calibration coefficient (primary standard to secondary standard ratio) is calculated.

The last term of Equation 33 is the air temperature and pressure correction, k_{TP}, where

T is the ambient temperature (K) and

p is the ambient atmospheric pressure (kPa).

Inserting all calculated factors in Equation 33 gives the following shortened version. The RAKR of an HDR ^{192}Ir source is

$$\dot{K}_R = \left(I_{raw} - I_{leakage}\right) \cdot k_{elec} \cdot k_{ion} \cdot \left(\frac{d}{d_{ref}}\right)^2 \cdot k_{air} \cdot k_{dec} \cdot k_{TP} \cdot 2.8772 \cdot 10^5 \text{ Gy/C}. \qquad (36)$$

The total uncertainty of the source calibration is 0.7% (k = 2). A summary of the uncertainty analysis follows in chapter 7.

7 Summary of uncertainty analysis

The uncertainty analysis tables listed on the next three pages[3] were written following the recommendations given in the Guide to the Expression of Uncertainty in Measurement (GUM) (ISO 1995).

The symbols used in the column headers are those introduced by Bentley (2005).

U_i represents a raw estimate of uncertainty of the i^{th} input quantity and
k_i is the reducing factor needed to convert the expanded uncertainty U_i to
$u(x_i) = U_i / k_i$ which is the standard uncertainty in the i^{th} input quantity.

All parameters in the measurement equation are input quantities apart from the measurand (the output quantity) and for each input quantity a sensitivity coefficient c_i is needed. The sensitivity coefficient expresses the effect on the measurand of a small change in an input quantity (approximately one standard deviation), while all other quantities remain fixed.
The effect on the measurand y (symbolised by δy_i) of a small change δx_i in the i^{th} input quantity x_i was determined analytically by applying the following equation:

$$\delta y_i = \left(\frac{\partial y}{\partial x_i} \right) \delta x_i = c_i \cdot \delta x_i \tag{37}$$

where $c_i = \partial y / \partial x_i$ is the sensitivity coefficient of the i^{th} input quantity. Some of the sensitivity coefficients listed in the uncertainty analysis table were determined using a numerical technique via the following equation expressed in words:

$$\text{sensitivity coefficient} = \frac{\text{resultant change in measurand}}{\text{small change in input quantity}} \quad . \tag{38}$$

$\left| c_i \cdot u(x_i) \right|$ is the uncertainty component and
u_c is the overall uncertainty (combined standard uncertainty) in the measurand, where

$$u_c^2 = \sum \left| c_i \cdot u(x_i) \right|^2 \quad . \tag{39}$$

v_i is the number of degrees of freedom and is a measure of how well each standard uncertainty had been estimated. The degrees of freedom for type B components (when other estimates were not available) were judged as being rough ($v_i = 3$), reasonable ($v_i = 10$) or good ($v_i = 30$).

[3] Re: Spreadsheet 'HDR brachytherapy uncertainty analysis (May 2006).xls'

v_{eff} is the effective degrees of freedom for the overall uncertainty in the measurement and is given by the Welch-Satterthwaite equation (Bentley 2005):

$$v_{eff} = \frac{u_c^4}{\sum_{i=1}^{N} \left| c_i \cdot u(x_i) \right|^4 / v_i} \tag{40}$$

where N is the number of input quantities. All other symbols were defined on the previous page. v_{eff} is needed in deriving a value for the coverage factor k and, thus, the expanded uncertainty. The coverage factor k, used in the ISO guide, is equal to Student's t value at the chosen coverage probability (95% is the value currently adopted internationally).

Table 14. Uncertainties in the primary standard corrections

Symbol	Quantity, source of uncertainty	Value of quantity	Expanded uncertainty U_i	Probability distribution	Coverage factor k_i	Standard uncertainty $u(x_i)$	Sensitivity coefficient c_i	Uncertainty component $\lvert c_i \cdot u(x_i) \rvert$	Degrees of freedom v_i	$\lvert c_i \cdot u(x_i) \rvert^4 / v_i$
k_{wall}	Wall correction	1.0453	±0.25%	normal	2	0.13	1.00	0.13	10	2.44E-05
k_{cel}	Central electrode correction	0.9984	±0.11%	normal	2	0.06	1.00	0.06	10	9.15E-07
k_{an}	Axial non-uniformity correction	0.9981	±0.22%	normal	2	0.11	1.00	0.11	10	1.46E-05
k_{rn}	Radial non-uniformity correction	1.0000	±0.04%	normal	2	0.02	1.00	0.02	10	1.60E-08
k_{stem}	Stem scatter correction	0.9983	±0.05%	normal	1	0.05	1.00	0.05	2	4.21E-06
k_{ion}	Ion recombination correction	1.0028	±0.02%	normal	1	0.02	1.00	0.02	10	3.32E-08
k_{pol}	Polarity correction	0.9983	±0.01%	normal	1	0.01	1.00	0.01	3	3.33E-09
k_h	Humidity correction	0.9970	±0.10%	normal	2	0.05	1.00	0.05	10	6.25E-07
$u_c(F)$	Combined standard uncertainty			normal	1			0.19		
U	Expanded uncertainty			normal	2			0.39		

Table 15. Uncertainties in the primary standard measurement

Symbol	Quantity, source of uncertainty	Value of quantity	Expanded uncertainty U_i	Probability distribution	Coverage factor k_i	Standard uncertainty $u(x_i)$	Sensitivity coefficient c_i	Uncertainty component $\lvert c_i \cdot u(x_i)\rvert$	Degrees of freedom ν_i	$\lvert c_i \cdot u(x_i)\rvert^4 / \nu_i$
F	Total primary standard correction	1.0379	±0.19%	normal	1	0.19	1.00	0.19		
k_{elec}	Electrometer charge calibration	1.000	±0.19%	normal	2	0.10	1.00	0.10	10	8.15E-06
k_{res}	Electrometer resolution (nC)	0.0005	±0.05%	rectangular	1.732	0.03	1.00	0.03	10	6.94E-08
t	Time (s)	60	±0.10%	rectangular	1.732	0.06	-1.00	0.06	10	1.11E-06
$I_{leakage}$	Leakage current (A)	1E-14	±0.05%	normal	1	0.05	1.00	0.05	3	2.08E-06
$S_{air}^{graphite} \cdot k_{fl}$	Mass stopping power ratio (graphite to air) x fluence perturbation correction	1.0082	±0.25%	normal	2	0.13	1.00	0.13	10	2.44E-05
W_{air}/e	Energy per ion pair (J/C)	33.97	±0.05% *)	normal	1					
$(\mu_{en}/\rho)_{graphite}^{air}$	Mass energy absorption coefficient ratio (air to graphite)	1.0016	±0.22%	normal	2	0.11	1.00	0.11	10	1.46E-05
$1/(1-g)$	Fraction of energy lost by bremsstrahlung	1.0007	±0.03%	normal	2	0.02	1.00	0.02	10	5.06E-09
ρ_{air}	Density of dry air (kg/m^3)	1.2045	±0.01%	normal	1	0.01	-1.00	0.01	30	3.33E-10
$\rho_{graphite}$	Density of high purity graphite (kg/m^3)	1750	±1.70%	normal	2	0.85	0.05	0.04	10	2.20E-07
T	Temperature (K)	293.15	±0.14%	normal	2	0.07	-1.00	0.07	3	8.98E-06
p	Pressure (kPa)	101.33	±0.04%	normal	2	0.02	1.00	0.02	10	2.32E-08
V ,	Volume of cavity (cm^3)	102.52								
d_{sphere}	Internal diameter of sphere (mm)	58.03	±0.03 mm	normal	2	0.03	-3.00	0.09	10	6.56E-06
$V_{insulator}$	Volume of protruding insulator (mm^3)	0	±5.65 mm^3	normal	2	0.01	-1.00	0.01	3	2.08E-10
V_{gap}	Volume change due to variation in gap width (mm^3)	0	±36.0 mm^3	rectangular	1.732	0.02	-1.00	0.02	3	9.48E-08
$R_{angular}$	Angular response change		±0.15%	rectangular	1.732	0.09	1.00	0.09	10	5.63E-06
R	Repeatability		±0.03%	normal	1	0.03	1.00	0.03	14	5.79E-08
$u_c(K_a)$	Combined standard uncertainty			normal	1			0.32		
U	Expanded uncertainty			normal	2			0.65		

*) Due to correlated uncertainties between the stopping power ratio and W_{air}/e, the uncertainty in W_{air}/e has been included in the combined uncertainty for the product $S_{air}^{graphite} \cdot W_{air}/e \cdot k_{fl}$.

Table 16. Uncertainties in the calibration of the source

Symbol	Quantity, source of uncertainty	Value of quantity	Expanded uncertainty U_i	Probability distribution	Coverage factor k_i	Standard uncertainty $u(x_i)$	Sensitivity coefficient c_i	Uncertainty component $\lvert c_i \cdot u(x_i) \rvert$	Degrees of freedom v_i	$\lvert c_i \cdot u(x_i) \rvert^4 / v_i$
K_a	Primary standard measurement		±0.32%	normal	1	0.32	1.00	0.32		
k_{aasc}	Air attenuation and scatter correction	1.0158	±0.02%	normal	1	0.02	1.00	0.02	30	5.33E-09
k_{dec}, Decay correction										
$\tau_{1/2}$	Half-life of ^{192}Ir (days)	73.827	±0.013 d	normal	1	0.02	-0.84	0.02	30	2.66E-09
t_{now}	Time of measurement	hh:mm	±2 min	rectangular	1.732	0.08	0.01	0.00	30	1.42E-14
d, Centre-to-centre source-chamber distance (mm)		1433								
d_{pos}	Catheter position	0	±0.5 mm	normal	2	0.02	2.00	0.02	3	5.33E-08
d_{source}	Source position in catheter	0	±0.2 mm	binary	1	0.01	2.00	0.03	30	2.05E-08
$d_{cath-ap}$	Catheter to back of aperture	299	±0.1 mm	normal	2	0.00	2.00	0.01	10	2.40E-10
$d_{ap-cham}$	Front of aperture to chamber	1020	±0.1 mm	normal	2	0.00	2.00	0.01	10	2.40E-10
S_{lat}	Lateral source positioning		±1 mm	normal	2	0.03	0.00	0.00	30	0.00E+00
S_{spec}	Source spectrum		±0.20%	normal	2	0.10	1.00	0.10	3	3.33E-05
A	Source alignment in catheter		±2 deg	rectangular	1.732	0.01	0.00	0.00	10	0.00E+00
$u_c(\dot{K}_R)$	Combined standard uncertainty			normal	1			0.34		
							$u_c^4 =$	0.01		
							$v_{eff} =$	91		
							$k =$	1.99		
U	Expanded uncertainty			normal	2			0.68		

8 Acknowledgements

The authors would like to thank Martin Kelly and Andy Shah for carrying out various measurements to determine the polarity correction, stem scatter correction and ion recombination correction. We also wish to thank Dr Simon Duane and Dr Hugo Palmans for their valuable suggestions and discussions and for carefully reading the manuscript. Finally, we wish to acknowledge the work of Michael Parfitt of NPL Engineering Services who designed the lead collimator and Nigel Cross of CBTLM who measured most of the dimensions of the graphite sphere and the central electrode of the ionisation chamber.
The authors also acknowledge the financial support of the National Measurement System Policy Unit of the UK Department of Trade and Industry.

9 References

Aird E G A, Jones C H, Joslin C A F, Klevenhagen S C, Rossiter M J, Welsh A D, Wilkinson J M, Woods M J and Wright S J 1993 Recommendations for brachytherapy dosimetry *Report of a Joint Working Party of the BIR and IPSM* (London: BIR) 1-17

Attix F H 1986 Introduction to radiological physics and radiation dosimetry, A Wiley-Interscience Publication, John Wiley & Sons, New York, Chichester, Brisbane, Toronto, Singapore

Attix F H 1984 Determination of A_{ion} and P_{ion} in the new AAPM radiotherapy dosimetry protocol *Med. Phys.* **11** 714-716

BAM 2002 Approval certificate for the design of a "special form radioactive material" D/0046/S-96 (Rev. 4), Bundesanstalt für Materialforschung und –prüfung (BAM), Berlin, Germany

Bentley R E 2005 Uncertainty in Measurement: The ISO Guide, Monograph 1: NMI Technology Transfer Series, tenth edition, National Measurement Institute, Australia

Boag J W 1987 Ionization chambers pp 169-243 In: Kase K R, Bjärngard B E and Attix F H (eds.), The dosimetry of ionizing radiation, Vol. II, Academic Press, Inc., Orlando, Florida

Boutillon M 1998 Volume recombination parameter in ionization chambers *Phys. Med. Biol.* **43** 2061-2072

Boutillon M and Perroche-Roux A M 1987 Re-evaluation of the W for electrons in Dry Air *Phys. Med. Biol.* **32** 213-219

Boutillon M and Perroche A M 1985 Effect of a change of stopping-power values on the W value recommended by ICRU for electrons in dry air, Comité Consultatif

pour les Étalons de Mesure des Rayonnements Ionisants (CCEMRI) Section I/85-8, Bureau International des Poids et Mesures (BIPM), Sèvres

BT1 1998 Experimental book 'HDR Brachytherapy BT1 1998 – 2004', pp 229-232 and pp 243-245

BT2 2004 Experimental book 'HDR Brachytherapy BT2 2004 – 200x', pp 38-41

Büermann L, Kramer H-M, Schrader H and Selbach H-J 1994 Activity determination of ^{192}Ir solid sources by ionization chamber measurements using calculated corrections of self-absorption *Nucl. Instr. and Meth. in Phys. Res. A* 339 369-376

COMSOL A B 2005 Comsol Multiphysics^{TM} Reference Manual Version 3.2 (Stockholm: Comsol AB)

Das R K and Thomadsen B R 2005 High Dose Rate Sources and Delivery Systems pp 59-74 In: Thomadsen B R, Rivard M J and Butler W M (eds.), Brachytherapy Physics, Second Edition, American Association of Physicists in Medicine, Medical Physics Monograph No. 31, Medical Physics Publishing, Madison, WI

Davis R S 1992 Equation for the Determination of the Density of Moist Air (1981/91) Metrologia **29** 67-70

DDEP 2005 Decay Data Evaluation Project: BNM-CEA/LNHB (France), PTB (Germany), INEEL (USA), KRI (Russia), LBNL (USA), NPL (United Kingdom), CIEMAT (Spain). http://www.nucleide.org/DDEP.htm, accessed January 2006

Douysset G, Gouriou J, Delaunay F, DeWerd L, Stump K and Micka J 2005 Comparison of dosimetric standards of USA and France for HDR brachytherapy *Phys. Med. Biol.* **50** 1961-1978

Duane S, Bielajew A F and Rogers D W O 1989 Use of ICRU-37/NBS Collision Stopping Powers in the EGS4 System, National Research Council, Canada, PIRS-0173

Goetsch S J, Attix F H, Pearson D W and Thomadsen B R 1991 Calibration of ^{192}Ir high-dose-rate afterloading systems *Med. Phys.* **18** 462-467

IAEA 2002 Calibration of photon and beta ray sources used in brachytherapy, International Atomic Energy Agency, IAEA-TECDOC-1274, Vienna

ICRU 1984 Stopping powers for electrons and positrons, ICRU Report 37, International Commission on Radiation Units and Measurements, Bethesda, MD

ICRU 1985 Dose and Volume Specification for Reporting Intracavitary Therapy in Gynecology, ICRU Report 38, International Commission on Radiation Units and Measurements, Bethesda, MD

ICRU 1997 Dose and Volume Specification for Reporting Interstitial Therapy, ICRU Report 58, International Commission on Radiation Units and Measurements, Bethesda, MD

ISO 1995 Guide to the expression of uncertainty in measurement, International Organization for Standardization, Geneva

ISO 1979 X and gamma reference radiations for calibrating dosemeters and dose ratemeters and for determining their response as a function of photon energy, ISO Standard 4037:1979, International Organization for Standardization, Geneva

Kawrakow I 2000 Accurate condensed history Monte Carlo simulation of electron transport. I. EGSnrc, the new EGS4 version *Med. Phys.* **27** 499-513

Loftus T P 1980 Standardization of iridium-192 gamma-ray sources in terms of exposure *J. Res. Natl. Bur. Stds.* **85** 19-25

Nelson W R, Hirayama H and Rogers D W O 1985 The EGS4 Code System, Report SLAC-265, Stanford Linear Accelerator Center, Stanford, CA 9430

Petersen J J, van Dijk E and Aalbers A H L 1994 Comparison of methods for derivation of ^{192}Ir calibration factors for the NE 2561 & 2571 ionisation chambers, Report S-El-94.01, NMi Van Swinden Laboratorium, Utrecht, The Netherlands

Raso D J 1963 Monte Carlo Calculations on the Reflection and Transmission of Scattered Gamma Rays, Nucl. Sci. and Eng. **17** 411-418

Rogers D W O and Ross C K 1988 The role of humidity and other correction factors in the AAPM TG-21 dosimetry protocol *Med. Phys.* **15** 40-48

Rogers D W O, Duane S, Bielajew A F and Nelson W R 1989 Use of ICRU-37/NBS Radiative Stopping Powers in the EGS4 System, National Research Council, Canada, PIRS-0177

Rogers D W O, Faddegon B A, Ding G X, Ma C-M, Wei J and Mackie T R 1995 BEAM: A Monte Carlo code to simulate radiotherapy treatment units. *Med. Phys.* **22** 503-524

Seltzer S M and Bergstrom P M 2003 Changes in the U.S. Primary Standards for the Air Kerma From Gamma-Ray Beams *J. Rs. Natl. Inst. Stand. Technol.* **108** 359-381

Stump K E, DeWerd L A, Micka J A and Anderson D R 2002 Calibration of new high dose rate ^{192}Ir sources *Med. Phys.* **29** 1483-1488

Takata N, Tran N T, Kim E, Marsoem P, Kurosawa T and Koyama Y 2005 Loss of ions in cavity ionization chambers Appl. Radiat. Isot. **63** 805-808

10 Appendices

10.1 Description of the Nucletron microSelectron HDR Classic ^{192}Ir source

The brachytherapy radiation source used at the National Physical Laboratory for the HDR brachytherapy calibration service and for the experimental and theoretical determination of the primary standard correction factors is a Nucletron microSelectron Classic source, part number: 096.001, manufactured by Mallinckrodt Medical B. V., The Netherlands (BAM 2002). The enclosure of the radioactive material consists of a cylindrical stainless steel AISI 316L capsule (length: 5.0 mm, radial thickness: 250 μm) which is sealed by laser welding (see Figure 28). The ^{192}Ir is contained in the capsule as a metallic ^{192}Ir cylinder (length: 3.5 mm, diameter: 0.6 mm). The stainless steel capsule is welded to a metal plug and a 1500 mm long flexible stainless steel AISI 316 cable. The other end of the capsule is welded to a steel pin (tail). The identification of the source is engraved on the long side of the tail. The nominal initial activity of the source is between 370 GBq and 550 GBq.
Figure 28 shows a schematic diagram of the 192Ir source currently used at the NPL.

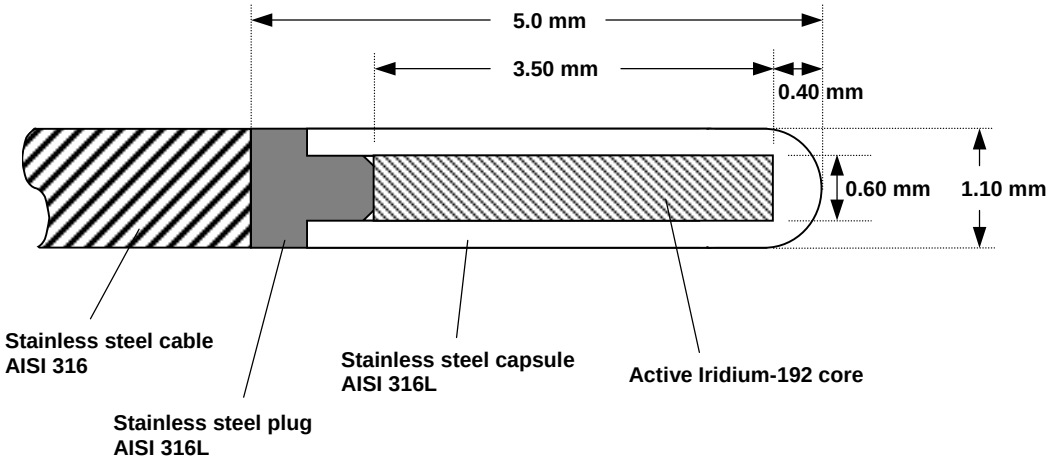

Figure 28. Schematic diagram of the Nucletron microSelectron HDR Classic ^{192}Ir source

10.2 Comparison with BNM-LNHB

In 2004/05 four secondary standard ionisation chambers for HDR ^{192}Ir sources were calibrated at the French standards laboratory, BNM-LNHB, and the UK standards laboratory, NPL. The purpose of this bilateral comparison was to validate the new NPL primary standard and to compare it to today's international consensus. One method of disseminating HDR brachytherapy dosimetric standards to users (medical physicists) is via well-type transfer ionisation chambers. The comparison was based on cross calibrations of four of these chambers. The results of the comparison have not been published yet.
BNM-LNHB used an indirect method, in which the RAKR of the source was measured with a cavity ionisation chamber using a technique originally developed by Goetsch *et al.* in 1991. Several improvements have been implemented in order to reduce the uncertainty levels. The calibration coefficient of the cavity ionisation

chamber for the ^{192}Ir spectrum was determined indirectly by interpolation from X-rays (250 kVp), ^{137}Cs and ^{60}Co national references.
NPL used the new primary standard cavity chamber to measure the RAKR of the ^{192}Ir source.
Two different brachytherapy sources were used by the two laboratories to calibrate the four well chambers. NPL used the Nucletron microSelectron Classic ^{192}Ir source as described in section 10.1. The LNHB used a Nucletron microSelectron HDR V2 source. This source was similar to the 'Classic' source, however, the dimensions of the active iridium core were as follows: length = 3.6 mm, diameter = 0.65 mm. The ^{192}Ir cylinder was surrounded by an AISI 316L stainless steel encapsulation (0.90 mm diameter).
The well chambers were positioned at least 1 m from any wall and 1 m above floor level on a low scatter surface. Before commencing measurements, sufficient time was allowed for the chamber to reach thermal equilibrium with the surrounding air. The well chamber was connected to a calibrated electrometer. Measurements were taken after a warm-up period of at least 30 minutes in which time the electrometer, ionisation chamber and cables were allowed to settle.
The point of maximum response (sweet-spot) of the chamber was found by stepping the ^{192}Ir source through the chamber and by plotting the corrected ionisation current versus the dwell position of the source. The ^{192}Ir source was then sent to the dwell position corresponding to the maximum chamber response and two sets of ten measurements of the ionisation current were taken. The electrometer correction factor was applied and all currents were corrected to the same reference date and time as used during the RAKR measurement by applying a decay correction. The calibration coefficient was normalised to standard atmospheric conditions, T_0 = 293.15 K and p_0 = 101.325 kPa. The well chamber calibration coefficient was obtained by applying the following equation:

$$N_{\dot{K}_R} = \frac{\dot{K}_R(t_{ref})}{I_{raw} \cdot k_{elec} \cdot k_{dec} \cdot k_{ion}} \tag{41}$$

where $\dot{K}_R(t_{ref})$ is the source RAKR (Gy/s) measured at the chosen reference time t_{ref}, I_{raw} is the measured current, corrected for leakage and atmospheric effects (A), k_{elec} is the electrometer correction factor and k_{dec} is the decay correction between the source calibration and the well-chamber calibration and $k_{ion} = (A_{ion})^{-1}$ is the recombination correction factor which is the inverse of the charge collection efficiency (Attix 1984).

Table 17. Results of the HDR brachytherapy comparison between NPL and LNHB (2004/05)

Owner	NPL	NPL	LNHB	LNHB
Well chamber type	PTW 33004	Standard Imaging 1000Plus	Nucletron SDS	Standard Imaging 1000Plus
Serial number	0031	A961699	25324	A002231
Collected charge	positive	negative	negative	negative
Calibration coefficient (LNHB)	2.513E+2 Gy/C	1.286E+2 Gy/C	2.592E+2 Gy/C	1.285E+2 Gy/C
Calibration coefficient (NPL)	2.501E+2 Gy/C	1.278E+2 Gy/C	2.580E+2 Gy/C	1.278E+2 Gy/C
Ratio of calibration coefficients NPL/LNHB (%)	-0.44%	-0.67%	-0.46%	-0.56%

The total expanded uncertainty ($k = 2$) of the well chamber calibration coefficients in terms of Gy/C was quoted as 1.3% (LNHB) and 0.8% (NPL).
All these comparisons agreed within 0.44% - 0.67% which was within the measurement uncertainties.
After the comparison, the NPL correction factors for the primary standard chamber TH100C were revised (see main part of this report) resulting in a change of +0.17% in the chamber correction factor, i.e. the NPL calibration coefficients listed in Table 17 would be closer to the LNHB values.

10.3 Check of long term stability of primary standard

Since 2002 the long-term stability of the NPL primary standard TH100C has been checked by calibrating three reference ionisation chambers after each ^{192}Ir source change. For each reference chamber the running mean of the calibration coefficients in terms of Gy/C is calculated. The normalised calibration coefficients determined up to May 2006 are plotted in Figure 31, 32 and 33. From the measurements carried out until the publication of this report, it can be concluded that a variation of the calibration coefficients of ±0.4% from the running mean can be expected. If, after a source change, the calibration coefficient is found to be outside the ±0.4% range from the running mean, this needs to be investigated.

The following ionisation chambers have been established as NPL reference chambers:

Table 18. NPL reference chambers for HDR ^{192}Ir brachytherapy sources

Ionisation chamber	Type	Serial number
Well chamber	Standard Imaging 1000 Plus	A961699
Well chamber	PTW W33004	0031
Farmer-type thimble chamber with Nucletron source calibration jig (part number: 077.211)	NE2571	3272

Figure 29 shows a few well chambers suitable for measuring HDR sources. The source can be moved through a suitable transfer tube or a plastic catheter from the treatment head of the afterloader into the well chamber insert.

Figure 30 shows a thimble chamber clamped to the Nucletron source calibration jig. In the bottom right hand corner two transfer tubes can be seen which link the two catheters left and right of the thimble chamber to the brachytherapy treatment unit.

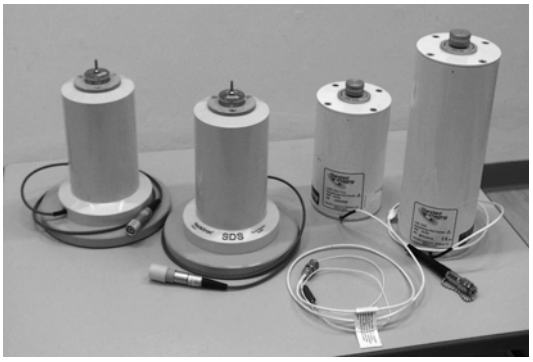

Figure 29. Well chambers for HDR brachytherapy sources

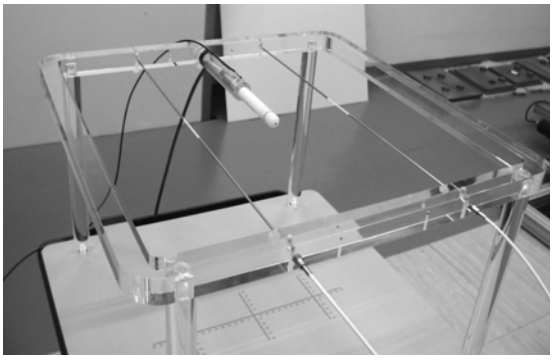

Figure 30. Thimble chamber and Nucletron Source Calibration Jig

10.3.1 Well chamber calibrations

The calibration is a two-step process: First, the RAKR of the Nucletron microSelectron Classic ^{192}Ir HDR source is determined using the NPL primary standard cavity chamber. The source is characterised in terms of Gy/s at 1 m.
Once the RAKR of the source is known, the ^{192}Ir source can be used to calibrate the reference ionisation chambers. The ionisation chamber is connected to a calibrated electrometer, the calibrated source is moved to the point of maximum response (sweet-spot) near the collecting volume of the chamber and the ionisation current is measured.

The calibration coefficient of the ionisation chamber, $N_{\dot{K}_R}$, is the ratio of the primary standard measurement of RAKR to the secondary standard measurement of ionisation current

$$N_{\dot{K}_R} = \frac{(\mathrm{Gy/s})}{(\mathrm{A})} = (\mathrm{Gy/C}). \tag{42}$$

The calibration procedure for a well chamber is described in section 10.2.
The total uncertainty of the well chamber calibration coefficient is 0.8% ($k = 2$).

10.3.2 Thimble chamber calibrations

The calibration procedure for thimble chambers is similar to the well chamber calibration procedure. When using the Nucletron Source Calibration Jig, the thimble chamber is set up between two catheters, such that the distance from the centre of the ^{192}Ir source to the centre of the thimble chamber is 100.0 mm ± 0.5 mm for both catheters (see Figure 30). The centre-to-centre distance from catheter 1 to catheter 2 is 200.0 mm ± 0.5 mm.

The point of maximum response (sweet-spot) of the thimble chamber is found by stepping the ^{192}Ir source through both catheters and by plotting the corrected ionisation current *versus* the dwell position of the source. The response curves look similar to a well chamber response curve. The ionisation current increases and then decreases when the source is moved through the catheter parallel to the long axis of the chamber (see Figure 30). The corrected ionisation current at the sweet-spot is calculated for both channels and the average current, $\bar{I}_{raw}$, is used for the calculation of the calibration coefficient, $N_{\dot{K}_R}$, again in terms of Gy/C, where

$$N_{\dot{K}_R} = \frac{\dot{K}_R(t_{ref})}{\bar{I}_{raw} \cdot k_{elec} \cdot k_{dec}} \quad . \tag{43}$$

The recombination correction for thimble chambers measuring HDR ^{192}Ir sources is negligible and therefore not applied.

The total uncertainty of the thimble chamber calibration coefficient is 1.1% ($k = 2$). This is greater than the uncertainty quoted for well chamber calibration coefficients, which is mainly due to the positional uncertainty in the set up of the thimble chamber in the calibration jig.

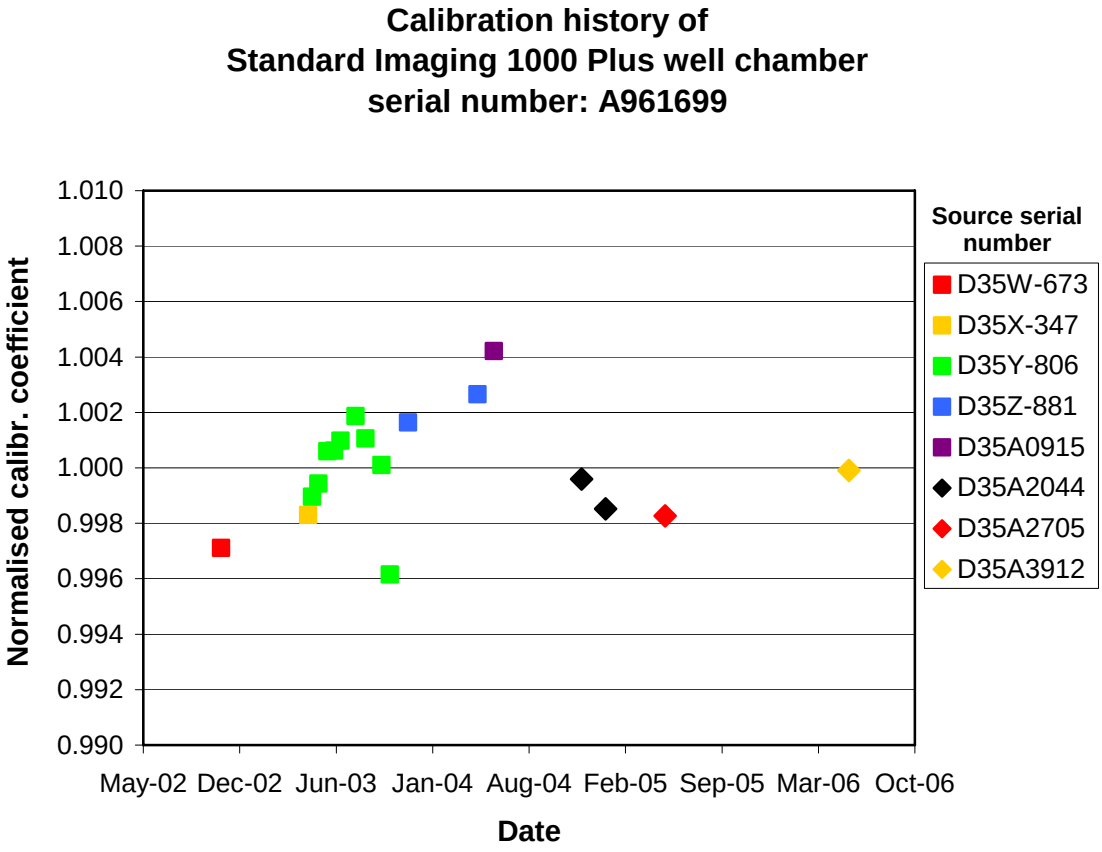

Figure 31. Normalised calibration coefficients of NPL reference chamber Standard Imaging 1000 Plus (serial number: A961699) versus calibration date.

The running mean of the calibration coefficients (recombination correction factor included) is 1.282E+2 Gy/C (September 2002 – May 2006).

Polarising potential: 300 V. Collecting electrode positive with respect to earth, i.e. negative charge collected.

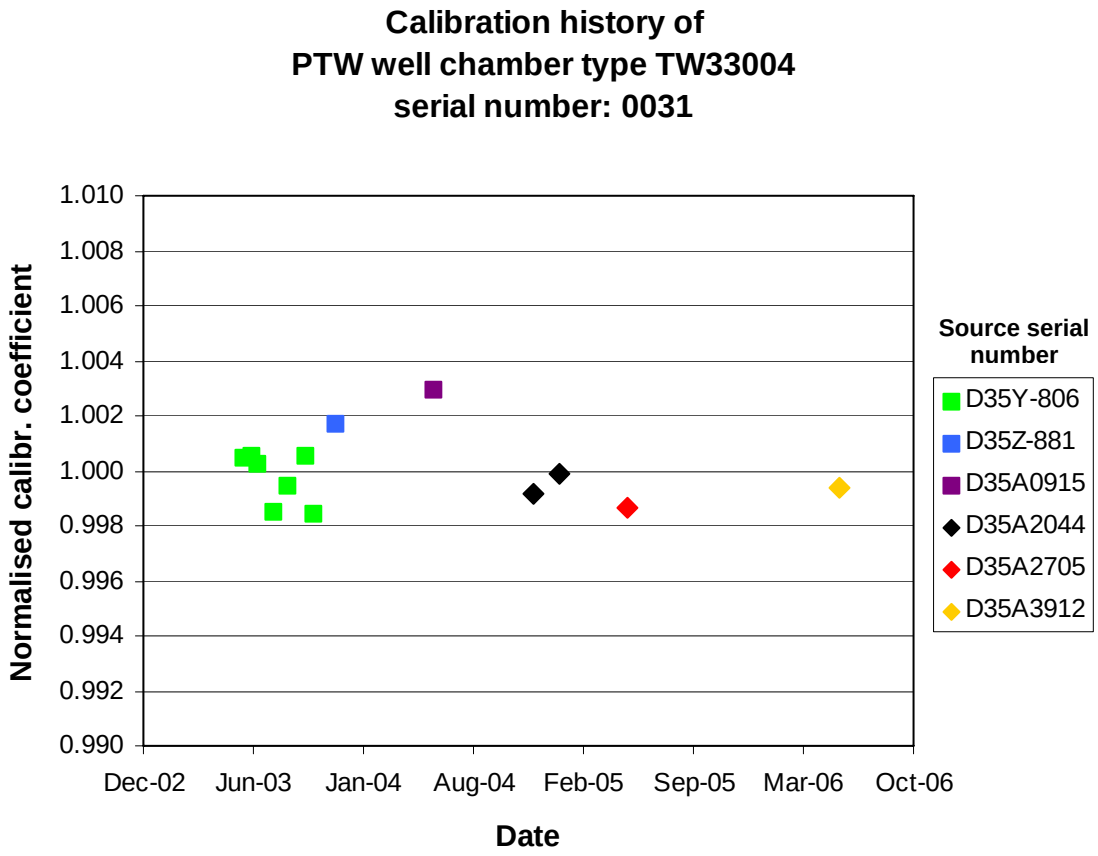

Figure 32. Normalised calibration coefficients of NPL reference chamber PTW TW33004 (serial number: 0031) versus calibration date.

The running mean of the calibration coefficients (recombination correction factor included) is 2.500E+2 Gy/C (June 2003 – May 2006).

Polarising potential: 300 V. Collecting electrode positive with respect to earth, i.e. negative charge collected.

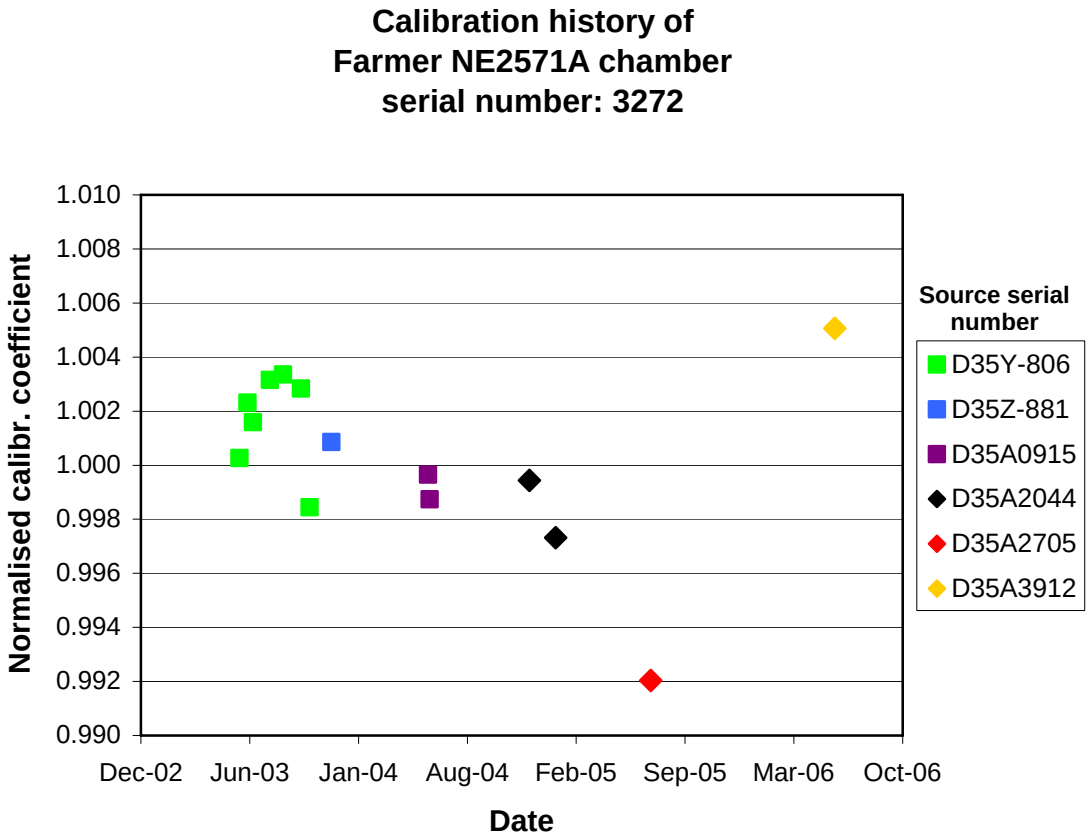

Figure 33. Normalised calibration coefficients of NPL reference chamber NE2571A (serial number: 3272) versus calibration date.

The running mean of the calibration coefficients is 4.143E+5 Gy/C (June 2003 – July 2005).
NB The last value determined in June 2006 was not included in the running mean due to repair of the calibration jig in May 2006.

In May 2006 both catheters of the calibration jig had to be replaced due to radiation damage in the old catheters. The whole set-up may have changed slightly. This may explain the 0.5% change of the calibration coefficient of the Farmer chamber.

All calibration coefficients were normalised to 200 mm catheter separation (centre-to-centre) and the calibration coefficient determined in June 2006 was compared with the previous running mean, i.e. (4.164E+5 Gy/C) / (4.143E+5 Gy/C) = 1.005.

A new calibration history will be started.

Polarising potential: 250 V. Collecting electrode positive with respect to earth, i.e. negative charge collected.